

Search for dark matter production in association with top quarks in the dilepton final state at $\sqrt{s} = 13$ TeV

Pablo Martínez Ruíz del Árbol, Jónatan Piedra Gomez, Cédric Prieëls
February 22th 2021

Instituto de Física de Cantabria

A search for the production of dark matter particles in association with either one or two top quarks is presented:

- We study the pp collisions produced by the LHC at $\sqrt{s} = 13$ TeV;
- Data collected by the CMS detector;
- Legacy analysis, considering the full Run II dataset (data collected in 2016, 2017 and 2018 and summing around 137 fb^{-1}).

Motivation

- Several (mostly astrophysical) evidences for the existence of dark matter, however **its nature remains unknown** and it has never been detected experimentally;
- If dark matter is made of some kind of particle it might be produced in the high energy collisions.

Main objective

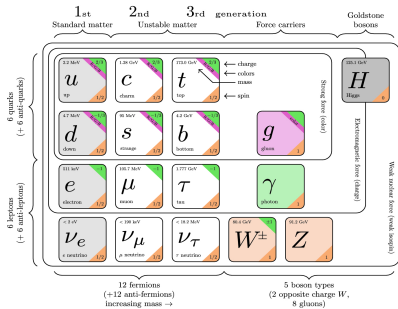
- Consider different dark matter production models to discover or eventually exclude some of them, or **put upper limits on their cross section of production**.

The dark matter case

The Standard Model

The most accepted model to describe the elementary particles and some of the fundamental interactions between them is the **Standard Model**:

- Contains 26 free parameters, among which the masses of the **12 predicted fermions**;
- Many **successful predictions** made over the years, such as the existence of the top quark, and the W, Z and Higgs bosons [?].



However, this model **has several shortcomings**: eventual exotic particles which do not fit within this model (such as dark matter) are extensively searched for nowadays.

At the origins of dark matter I

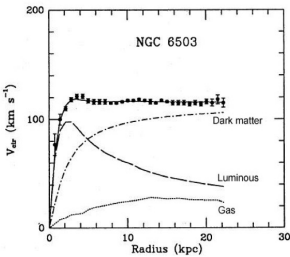
The concept of dark matter can be traced back to the 19th century, and was introduced to **explain several astrophysical evidences**, among which:

Zwicky's calculations

- Measurement of the mass of the Coma Cluster using the virial theorem;
- Concluded that its mass was **400-500 times larger** than the value obtained by Hubble, considering only visible galaxies.

Spiral galaxies rotation curves

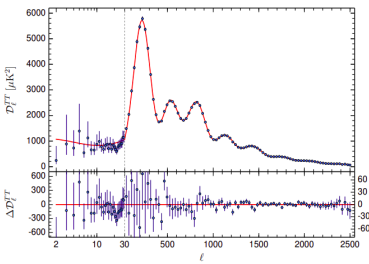
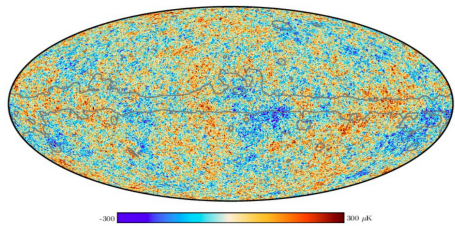
- Stars within spiral galaxies should rotate with a velocity depending on the radius to the galactic center, but **this is not what is observed experimentally**.
- Either our understanding of gravity at large scales or our basic understanding of galaxies as a celestial body made of stars has to be revised.



K.G. Begeman, A.H. Broeels, R.H. Sanders. 1991. Mon.Not.RAS 249, 523

CMB anisotropies

- Background of primary radio waves emitted when the Universe became transparent around 380 000 years after the Big Bang;
- Can be considered as emitting a black body spectrum with a temperature of $(2.72548 \pm 0.00057)\text{K}$, but small anisotropies at the 10^{-5} level are observed.
- Implies that dark matter **accounts for $\sim 27\%$ of the total mass of the Universe.**



Other observations, such as the gravitational lensing effect, **also tend to further support the existence of dark matter** (cf. backup).

Several fundamental properties of dark matter are nowadays known or assumed:

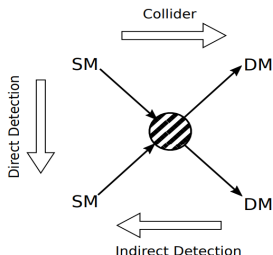
- Dark matter is a particle, given that it is assumed to have a certain mass;
- It should be dark, unable to interact with electromagnetic radiation, otherwise we would have seen it already. It should then also be electrically neutral;
- It is non-baryonic, because the energy density for the baryonic matter estimated from the CMB is too low to account for dark matter;
- We only consider cold dark matter since the widely accepted Λ_{CDM} model is based on this assumption and this helps explaining the presence of large scale structures in the Universe;
- It should have a mass in the electroweak scale, between 10 GeV and 1 TeV, because of the relic density obtained from the thermal freeze-out mechanism.
- Finally, it should be long-lived, since we expect them to have been produced during the Big Bang and they are still present in the Universe.

Weakly Interactive Massive Particles

The WIMPs are the dark matter candidates considered in this work, because of the so-called **WIMP miracle**. Indeed, they:

- Are expected to interact very weakly with ordinary baryonic matter;
- Have a mass in the 100 GeV-1 TeV range for reasonable electroweak production cross-section values;
- Give us a dark matter candidate while being able to solve the **hierarchy problem**.

Main search strategies



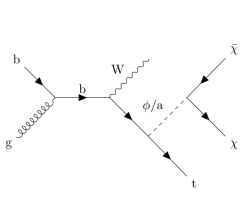
Different strategies are used:

- The **direct and indirect searches**, relying on the production of baryonic matter from the interaction between two DM particles or on the observation of the interaction between the dark and baryonic sectors;
- And the **collider production**, able to probe lower dark matter candidates masses.

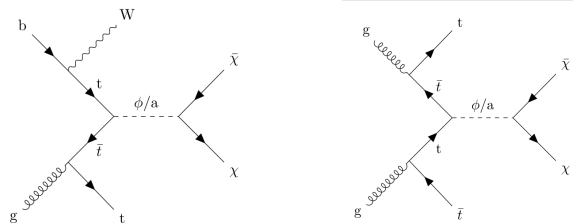
We are searching for **dark matter produced in association with either one or two top quarks**. Several **simplified models** are interesting to consider:

- Spin 1/2 DM χ ($\in [1, 55]$ GeV, Dirac fermion)
- Spin 0 scalar (S)/pseudoscalar (PS) mediator ϕ/a (Yukawa-like structure of such interactions → gain from the coupling of the mediator to top quarks)
- Mediator mass $\in [10, 1000]$ GeV
- Coupling g_χ mediator/DM set to 1 (same for all g_q couplings)

t/\bar{t} +DM tW models



$t\bar{t}$ +DM model



The **typical final state** of such models is made out of:

- 1 or 2 b-tagged jets coming from the decay of the top quark(s);
- 2 W bosons, seen as a combination of jets and leptons depending on the channel;
- Some MET coming from the dark matter and the decay of the Ws;

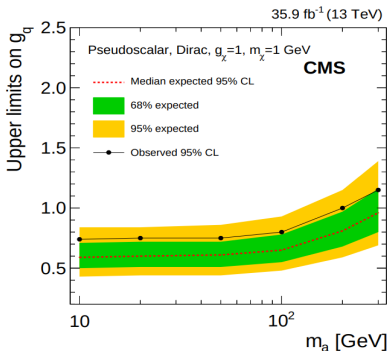
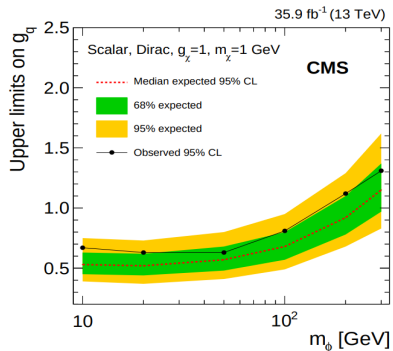
In particular, we are studying the **dilepton final state** in this work:

- Has the lowest branching ratio: $\text{BR}(W \rightarrow l^+ + \nu_l) = (10.80 \pm 0.09)\%$ for each of the three leptons (contains only 5% of the signal events);
- But, leptons can usually be reconstructed better than jets, resulting in lower systematic uncertainties;
- And this channel also has the lowest number of backgrounds, resulting in a better signal isolation.

This channel is then **expected to be competitive with the hadronic channel**, especially when considering high mediator masses, which feature a higher global discrimination signal/background.

Previous relevant results I

A similar analysis has already been published by CMS using 2016 data, considering the $t\bar{t}+DM$ signal only and a combination of the three possible final states.



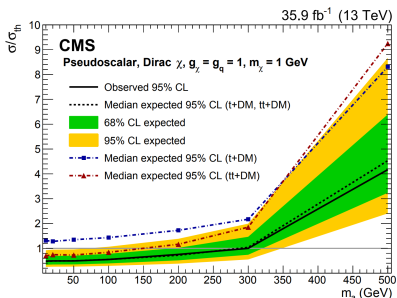
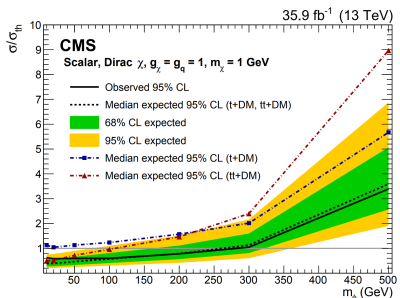
The observed (expected) limits excluded a **pseudoscalar mediator** with mass below 220 (320) GeV, and a **scalar mediator** with mass below 160 (240) GeV.

Previous relevant results II

A combination of both the $t/\bar{t}+DM$ and $t\bar{t}+DM$ processes has also been performed.

The inclusion of the single top signal process improved up to a factor 2 the limits obtained by the $t\bar{t}$ analysis on its own. This analysis:

- Only considered the 2016 data-taking period;
- And only considered the semi-leptonic and hadronic final states.



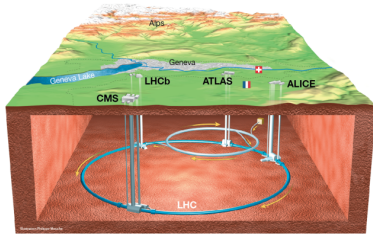
Scalar (pseudoscalar) mediators were with this combination excluded up to 290 (300) GeV at the 95% confidence level.

The experimental setup

The Large Hadron Collider

The data analyzed has been taken by the Large Hadron Collider:

- A 27 km circular underground proton-proton collider, located at CERN;
- Result of the collaboration of 22 countries;
- Built in order to study and reproduce the conditions of the Universe at its origin;
- Provided the collisions that lead to the discovery of the Higgs boson in 2012.
- Currently the most powerful accelerator in the world with its center of mass energy $\sqrt{s} = 13 \text{ TeV}$, therefore able to **scan new parts of the phase space**.



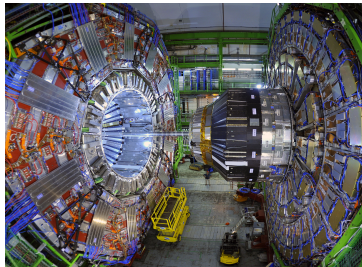
The data considered in this work has been collected during the **Run II of operation of the LHC** (from 2016 to 2018), at 13 TeV, totalling $(137.1 \pm 2.0) \text{ fb}^{-1}$ of data, selected by the different levels of trigger from the 40MHz collision rate.

The **Compact Muon Solenoid** is one of the two general purpose detectors of the LHC. Its main objectives consist in:

- Searching for and studying the properties of the Higgs boson;
- Trying to discover new BSM physics, such as the possible existence of dark matter.

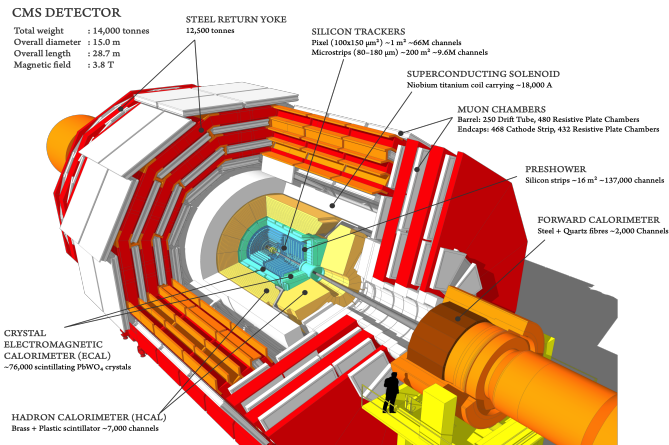
In a nutshell, CMS:

- Is a relatively **compact** (14.000 tons, distributed over a 15m diameter and a length of 8m) cylindrical detector;
- Is made out of a central part with cylindrical shape, the barrel, and two endcaps, one on each side in order to be **as hermetic as possible**, covering all the possible angles around the beam pipe;
- Has a **large solenoid** as middle piece, able to produce a 3.8T field;
- Features a **powerful tracker and muon detection system**.



The CMS detector II

The CMS detector is also **made out of different layers**, each having its own purpose, allowing for example to identify unequivocally each particle created.



Each subdetector of CMS has been designed carefully to fill its specific purpose:

- The **tracker** is the innermost piece of CMS, able to reconstruct the trajectories of charged particles issued from the interaction vertices in a quick and precise way;
- The **Electromagnetic CALorimeter**, enclosing the tracker system and able to give information about the energy of electrons and photons;
- The **Hadronic CALorimeter**, able to measure the energy of incident hadrons from the ionization process happening in its core;
- The 12.5 meters long and 6 meters large **solenoid**, allowing to measure precisely the charge and momentum of particles produced using the Lorentz effect, by measuring the curvature of their tracks;
- And finally, the **muon system**, covering more than $25\ 000\ m^2$ and made out of three different subsystems:
 - The **Drift Tubes** (DTs), in the barrel region;
 - The **Cathode Strip Chambers** (CSCs) in the two endcaps;
 - And the **Resistive Plate Chambers** (RPCs), mostly added to the barrel and to the endcap regions in order to cope with (in)ability of the previous muon system to identify unequivocally the correct bunch crossing when the LHC is running at full luminosity.

Global strategy

Analysis strategy

Run II legacy paper being worked on, expected to **combine both the $t/\bar{t}+DM$ and $t\bar{t}+DM$ searches**, and the 3 possible final states (hadronic, semi-leptonic and dileptonic).
→ Paper expected to be approved by LHCP (\sim June).

The effort is **globally common** between the groups studying the different final states:

- Objects are defined in a common way;
- Control and signal region orthogonal between the channels.
 - Number of leptons and b-jet categorization to improve the sensitivity by defining enriched $t/\bar{t}+DM/t\bar{t}+DM$ regions.

This talk will **be focused on the dilepton final state**, in which we are mostly involved, along with a team of DESY. Deborah Pinna and her team from the University of Wisconsin are focused on the semi-leptonic and hadronic channels.

Object and samples

We are currently using the following objects:

Triggers

- Single and double lepton triggers combined to gain statistics;
- Any possible double counting of events in multiple trigger is taken care of;
- Trigger p_T chosen to avoid any turn-on effect;
- SingleMuon, SingleEle, DoubleMuon, DoubleEG, MuonEG (2016) and SingleMuon, EGamma, DoubleMuon, MuonEG (2017/2018) data streams considered
- All the triggers used are listed in the backup.

Leptons

- Analysis relies on the selection of events with two leptons;
- Medium cut based POG WP used for electrons without additional ISO cut;
- Medium cut based POG WP for muons with tight ISO ($\text{pfRelIso04_all} < 0.15$)

Jets

- Clustered from the PF candidates using the **anti- k_T algorithm**;
- Basic selection: $p_T > 20$ GeV (30 for the leading jet), $|\eta| < 2.4$;
- **Tight JET/MET POG** working point (efficiency and background rejection $> 98\%$);
- Have to be $\Delta R > 0.4$ away from any lepton passing the criteria established for analysis to prevent signal leptons clustered as jets from entering the jet counting;
- Loose jet PU ID applied on top to reject jets coming from PU interactions.

B-tag

- B-Tagging and Vertexing POG **deep CSV b-tag medium working point** (high efficiency, misidentification rate for a light jet as a b-jet $\sim 10\%$);
- B-tagging weight larger than 0.6321, 0.4941 or 0.4184 (2016, 2017 or 2018).

MET

- **PfType1MET** considered by propagating the JECs to the MET;
- All recommended **MET filters applied** to filter anomalous high MET events due to several detector issues, such as eventual dead cells in the calorimeters;
- XY-shift (ϕ modulation fix) and EE noise (2017) corrections applied on top.

Data

Single/double leptons datasets built to avoid any eventual double counting, considering the 3 years of the Run II of operation of the LHC:

- $(35.9 \pm 0.9) \text{ fb}^{-1}$
- $(41.5 \pm 1.0) \text{ fb}^{-1}$
- $(59.7 \pm 1.5) \text{ fb}^{-1}$

A blinding policy is currently in place, allowing us to only look at 1 fb^{-1} of data per year near the signal regions.

Monte-Carlo

The major backgrounds have been considered from MC and read from NanoAOD. Each year has its corresponding MC samples:

- $t\bar{t}$: decaying to both 1 and 2 leptons;
- Single top: s, t and tW channels considered;
- Drell-Yan: HT-binned samples to increase the statistics, with a correction factor derived from data applied;
- TTZ and TTW: usually grouped together as TTV;
- Others: dibosons, tribosons, non-prompt contamination (data-driven, not MC).

Signal samples

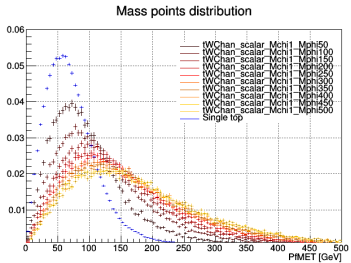
Both signal samples have been generated using MADGRAPH and PYTHIA8 (with the CP5 tune) at LO, while simulated events are then interfaced with a realistic model of the CMS detector using Geant4 [113] and are reconstructed using the official CMS reconstruction algorithms.

The $t/\bar{t}+DM$ process was **produced privately** (central request has been made but not processed), while the $t\bar{t}+DM$ was **generated centrally**. In both cases:

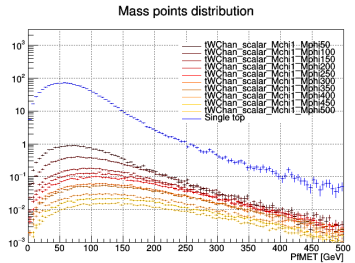
- Both scalar and pseudoscalar mediators are considered;
- 400.000 events were produced for each mediator mass, from 10 to 1000 GeV;
- The dark matter mass was set to 1 GeV, but additional samples ranging from 1 to 55 GeV were also produced;
- All the g_q and g_χ couplings were set to 1.

Scalar mediators

With normalization

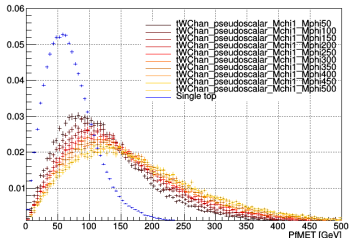


Without normalization

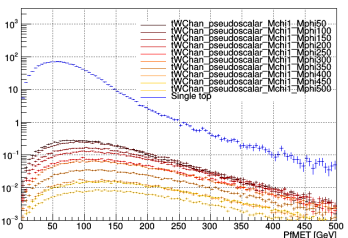


Pseudoscalar mediators

Mass points distribution

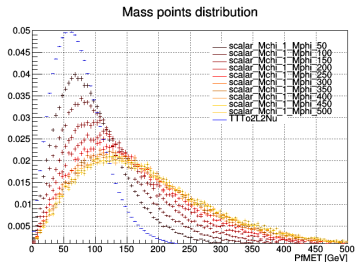


Mass points distribution

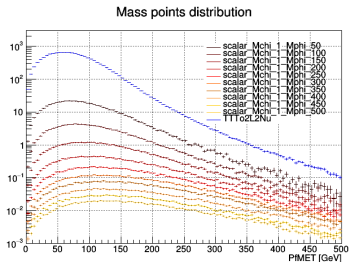


Scalar mediators

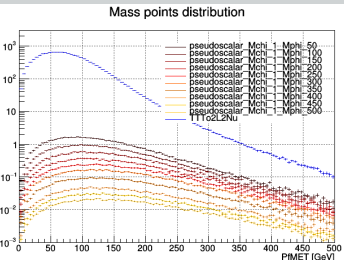
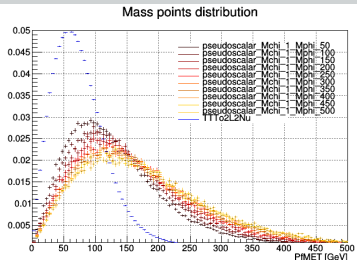
With normalization



Without normalization



Pseudoscalar mediators



Inclusive selection

Inclusive selection

First, distributions in the following inclusive control region mostly enriched in Drell-Yan were studied, in all the different channels available:

- Leading (trailing) lepton $p_T > 25$ (20) GeV
- Third lepton veto ($p_T < 10$ GeV)
- Opposite sign leptons
- $m_{\parallel} > 20$ GeV to avoid low mass resonances
- At least 1 jet
- At least 1 medium deep CSV b-jet

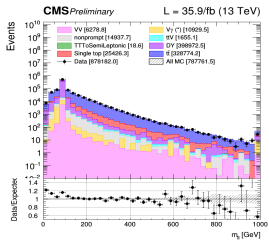
This region is studied to have a look at the most inclusive selection to spot initial issues and problems.

A slight mismodeling of the low mass DY+Jets sample and a general problem of the MET in DY events is observed, but these features are known in CMS and are mitigated with the analysis cuts applied.

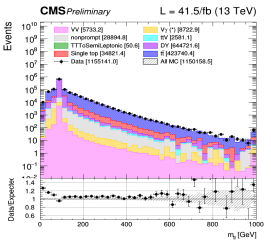
Inclusive control region

// channel

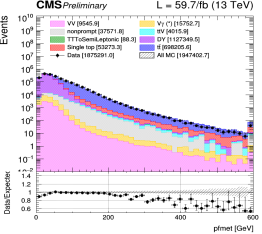
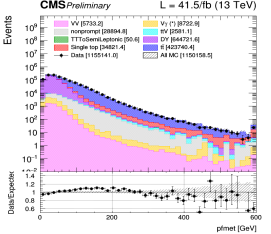
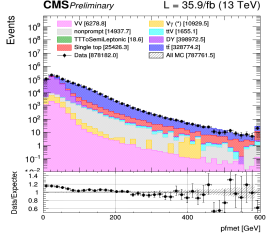
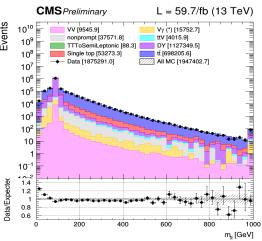
2016



2017



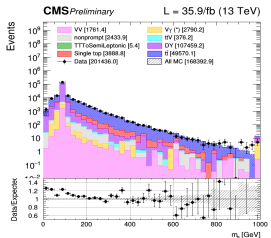
2018



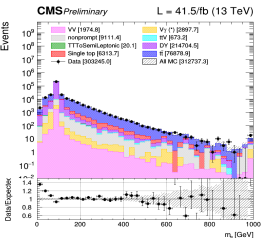
Inclusive control region

ee channel

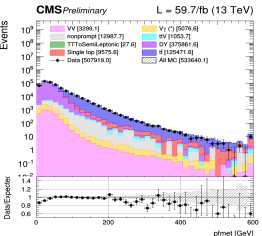
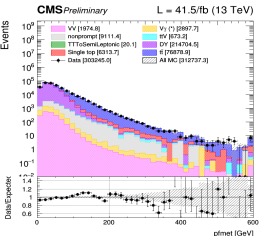
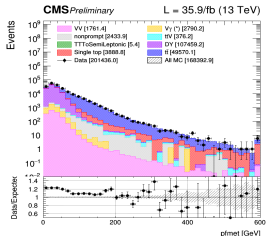
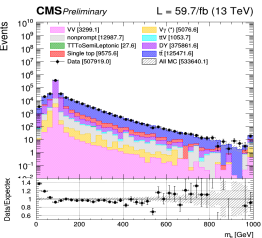
2016



2017

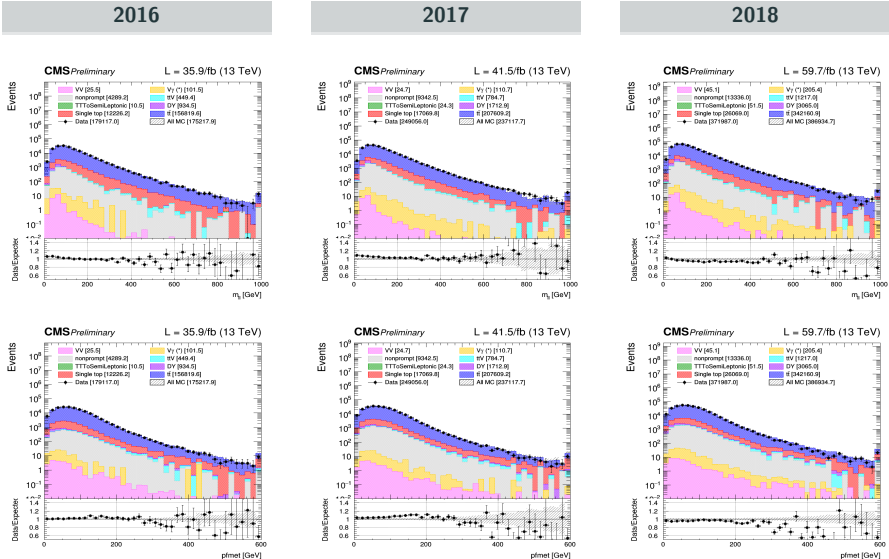


2018



Inclusive control region

df channel



Signal extraction

We trained both a BDT and an ANN, featuring the following common characteristics:

- Mix of standard model $t\bar{t}$ and single top as **backgrounds**, and mix of both $t/\bar{t}+DM$ and $t\bar{t}+DM$ as **signals**;
- Only events passing the **following pre-selection** are considered for the training:
 - 2 tight leptons: $p_T > 25, 20$ GeV
 - Third lepton: $p_T < 10$ GeV
 - Opposite sign leptons
 - $m_{ll} > 20$ GeV
 - 15 GeV Z-veto in ee and $\mu\mu$ channels
 - At least 1 jet
 - At least 1 b-jet
 - $M_{T2}^H > 80$ GeV, to stay orthogonal to the other channels
- One specific training performed per signal mass point;
- 50% train/test splitting used (~ 40.000 training events in total).

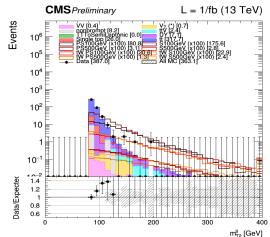
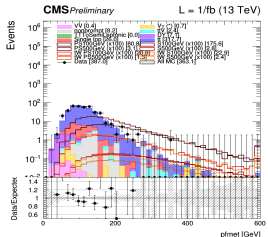
At the end of the day though, the **ANN was chosen for the analysis** over the BDT, given that it gave $\sim 10\%$ better upper limits once optimized. The ANN shape is then used to perform a general **shape analysis**.

The TMVA package was then finally used to study the training performed, as shown in the next few slides for the 2016 scalar 100/500GeV training performed. We plan on combining all the year together.

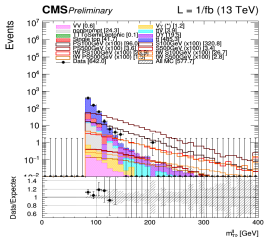
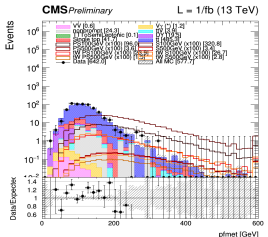
Pre-selection region

// channel

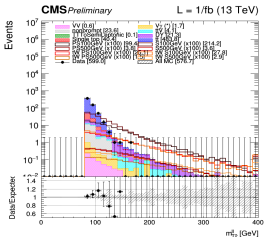
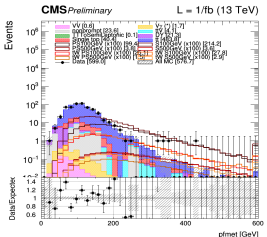
2016



2017



2018



Hyperparameters optimization

The hyperparameters of the ANN **have been fully optimized** one by one, trying each time to minimize the error in the test dataset and the discrimination obtained.

| DNN parameter | Optimized value |
|-----------------------|-----------------------------|
| Hidden layers neurons | 80, 80, 40 |
| Activation functions | Relu (x3), softmax (output) |
| Error function | Mean square error |
| Optimizer | Adam |
| Learning rate | 0.005 |
| Training epochs | 250 |
| Batch size | 250 |

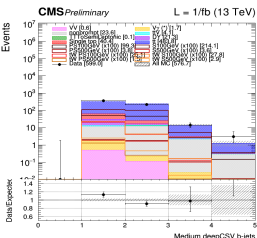
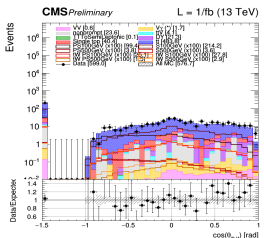
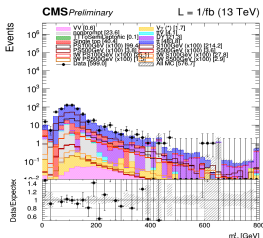
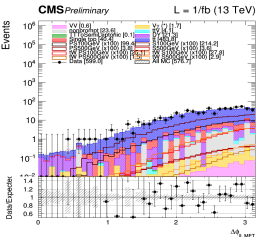
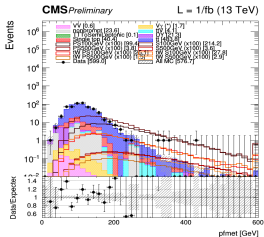
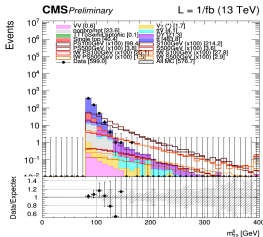
At the end of the day, the ANN using the following input variables was chosen:

| Rank | Variable | Importance |
|------|-------------------------------------|----------------------|
| 1 | M_{T2}^{ll} | $2.30 \cdot 10^{-1}$ |
| 2 | pfMET | $1.92 \cdot 10^{-1}$ |
| 3 | $\Delta\Phi(E_T^{\text{miss}}, ll)$ | $1.67 \cdot 10^{-1}$ |
| 4 | m_{bl}^t | $1.38 \cdot 10^{-1}$ |
| 5 | $\cos(\theta_i) \cos(\theta_j)$ | $1.35 \cdot 10^{-1}$ |
| 6 | nbJet | $6.95 \cdot 10^{-2}$ |

2018 discriminating variables

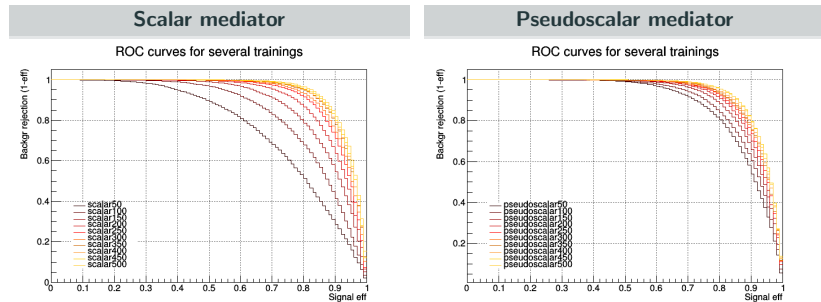
Example distributions shown in the blinded 2018 pre-selection region.

2018, // channel



ROC curves

ROC curves have been obtained for all the different mass points available, from 50 to 500 GeV, and for both scalar and pseudoscalar mediators.

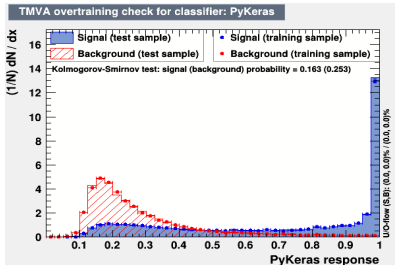


As expected, a better discrimination is achieved for higher mediator masses.

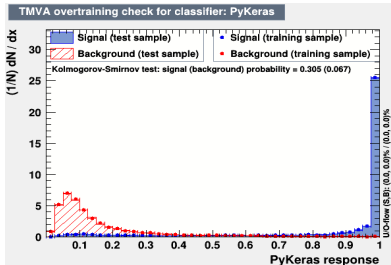
Overtraining plots

Scalar mediators

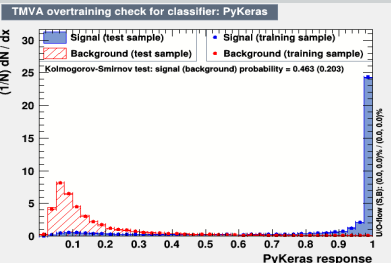
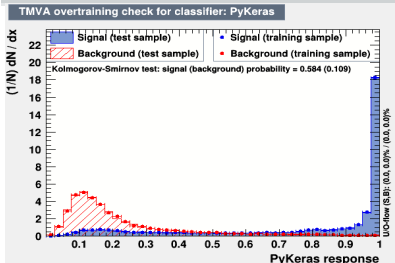
100 GeV



500 GeV

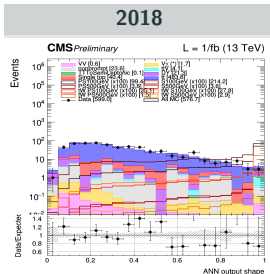
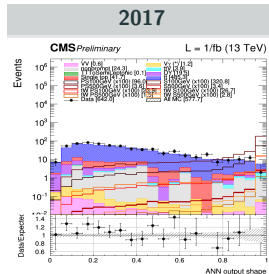
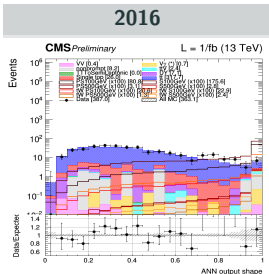


Pseudoscalar mediators

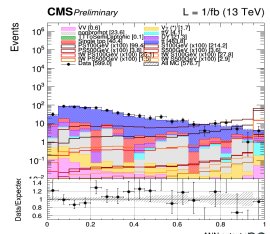
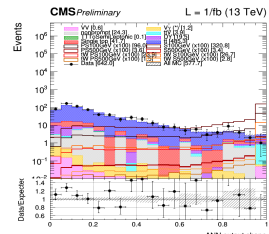
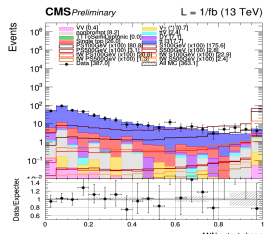


Blinded ANN output shape

Scalar 100 GeV output shape



Scalar 500 GeV output shape



Background prediction methods

Main background processes

The backgrounds are predicted either directly from Monte-Carlo simulations or from data-driven methods. In order of importance:

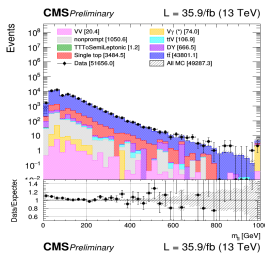
- The **$t\bar{t}$ and the single top** are taken from simulation accounting for all the variations in the generation parameters. Several parameters (QCD scale, PDF variation,...) are varied and included as a systematic (see later).
→ A data validation region (low M_{T2}^H) is explored to ensure the quality of the prediction;
- The **Drell-Yan** yields are obtained from a semi data-driven method using the excluded same flavor region on the Z peak as control region;
- The **non-prompt contamination** is estimated from data control regions and validated in a same sign validation region;
- The irreducible **ttV process** ($ttW + ttZ$) is taken from simulation and checked in a particular validation region;
- **Diboson processes and other minor backgrounds** are taken directly from MC.

Top control region

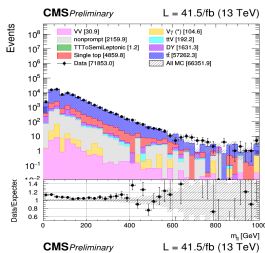
Same as the signal region but with $60 < M_{T2}^H < 80$ GeV.

// channel

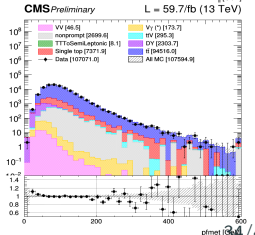
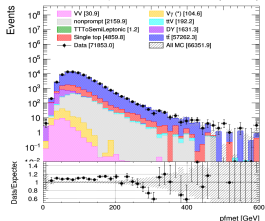
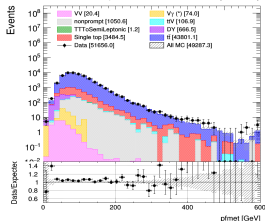
2016



2017



2018



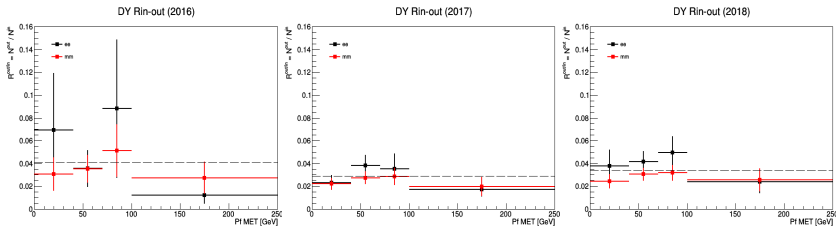
DY Rin-out method

We want to estimate the DY yields outside of the Z-peak from the data:

- Given the presence of large backgrounds (such as $t\bar{t}$) in the analysis region, we go inside of the Z-peak to compute the **Rin-out factor**:

$$N_{DY}^{out} = N_{DY, data}^{in} \cdot \kappa \cdot \left(\frac{N_{DY, MC}^{out}}{N_{DY, MC}^{in}} \right) \equiv N_{DY, data}^{in} \cdot \frac{R_{out/in, MC}^{0bj}}{R_{out/in, data}^{0bj}} \cdot R_{out/in, MC}$$

- To avoid any bias, the contamination of non-peaking backgrounds is removed and we correct this factor by the ratio κ between the data/MC transfer factors in a CR close to the SR (asking for 0 b-jet instead of 1);
- We then get this Rin-out in **bins of MET and for each channel (ee , $\mu\mu$) separately**:

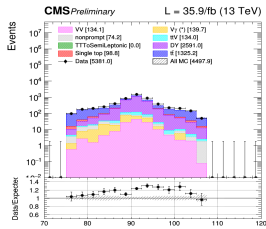


A flat scale factor and a fixed 20% systematic uncertainty is then applied to the DY. This method and the difference in statistics are still being studied.

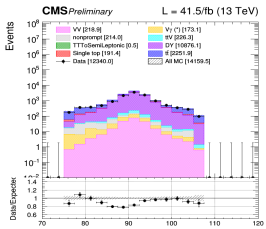
DY control region

// channel

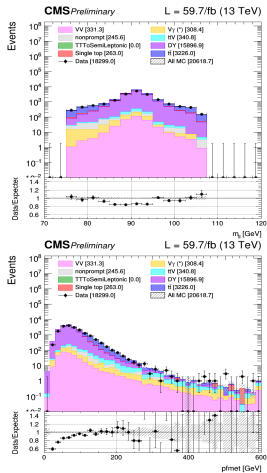
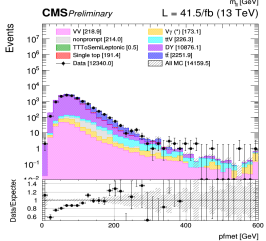
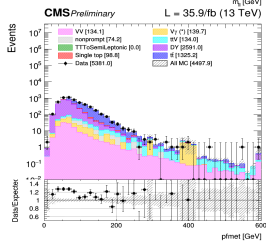
2016



2017



2018



The 0-bjet correction allows us to fix the data/MC discrepancies observed. A large systematic uncertainty is associated to this background, minor in the signal regions.

Non-prompt contamination I

Fake leptons detection (mostly jets misidentified or leptons coming from semileptonic b-quark decays $b \rightarrow cW \rightarrow cl\nu$) in the detector needs to be taken into account properly, through a **data-driven tight-to-loose method** since the Monte-Carlo is not reliable in this case:

Fake rate

- A QCD enriched region is defined with a looser particle selection criteria, where the misidentification should be high;
- Any eventual contamination from electroweak processes in this region is removed;
- The **fake rate** is defined as the ratio between the fakeable object (lepton-like objects passing only the loose isolation requirements) and fully selected objects yields.

Prompt rate

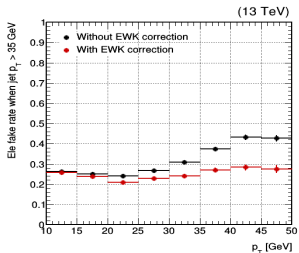
- The **prompt rate**, taking into account the real lepton contamination is calculated in a Z enriched region from a general tag and probe method.

Then, we calculate from data an extrapolation factor to go back to the signal region of the analysis and the results obtained are checked in a **same sign control region**.

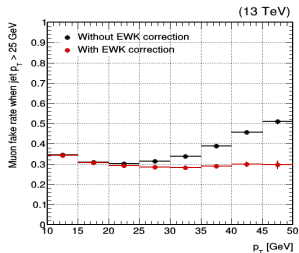
Non-prompt contamination II

2016 fake rate

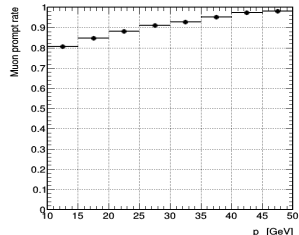
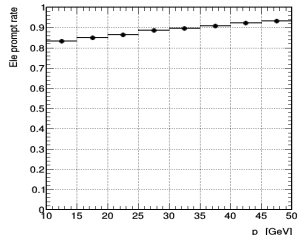
Electron



Muon



2016 prompt rate

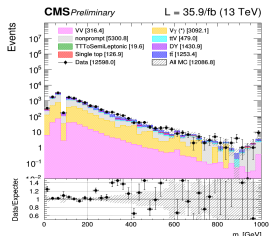


Same sign control region

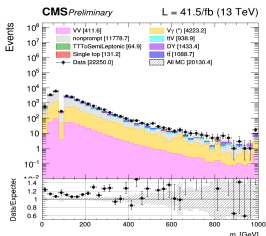
This is checked in a dedicated same sign control region.

// channel

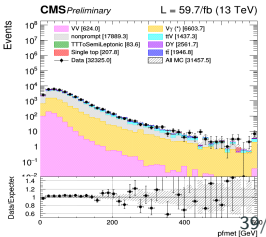
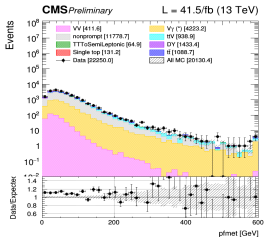
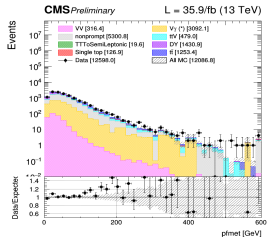
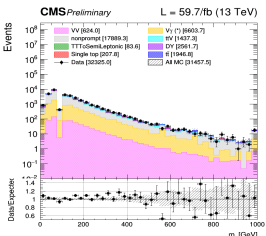
2016



2017



2018

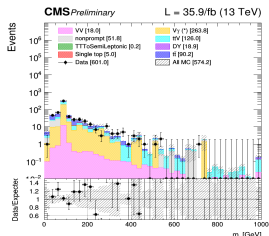


$t\bar{t}V$ prediction

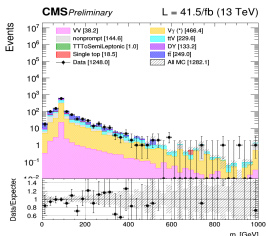
This process is taken directly from MC, and crosschecked in a dedicated control region.

// channel

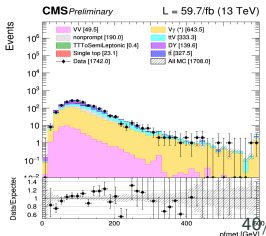
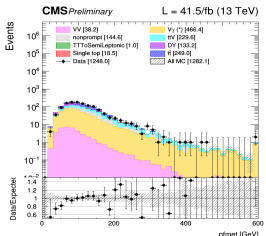
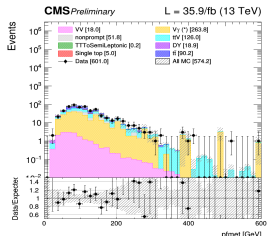
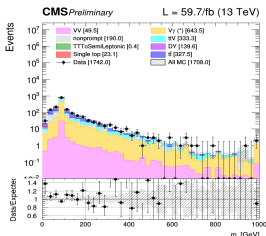
2016



2017



2018



Systematic uncertainties

Systematic uncertainties

Most of the systematics to be considered (on top of the statistical uncertainties) are already in place, such as:

Theoretical uncertainties

- PDF and higher order corrections, underlying event and parton shower, renormalization and factorization scales.

Experimental uncertainties

- Luminosity, pileup modeling, lepton trigger, lepton efficiency and energy scale, jet energy scale, MET mismodelling, b-tagging efficiency, top p_T reweighting.

Background specific uncertainties

- Drell-Yan and non-prompt backgrounds related uncertainties.

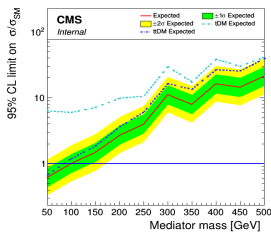
Disclaimer: this part of the analysis still needs to be checked/optimized, so results shown next do not include any systematics for now, even though we are mostly ready to include them when needed.

Results obtained

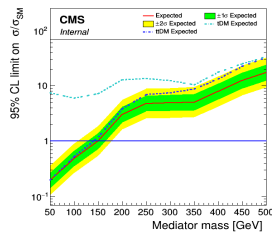
Upper limits without systematics

Scalar upper limits

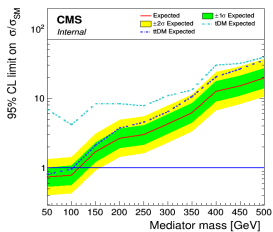
2016



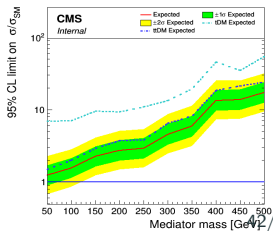
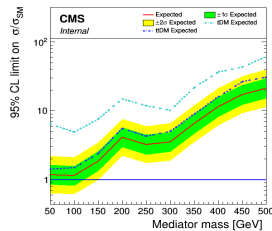
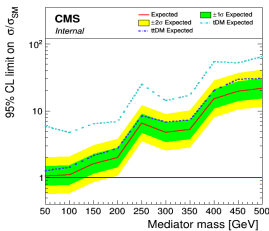
2017



2018

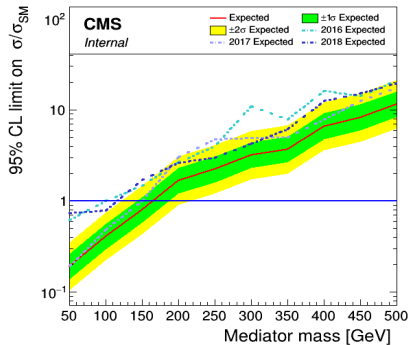


Pseudoscalar upper limits

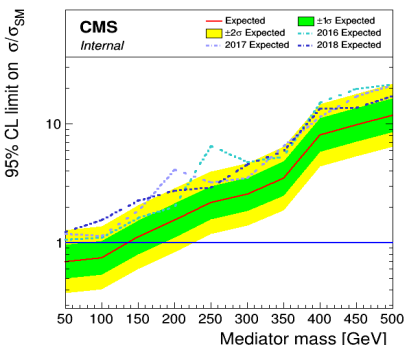


Disclaimer: comparison done without systematics and expected to change a bit.

Scalar mediators



Pseudoscalar mediators



Conclusions

A search for dark matter produced in association with either one or two top quarks is on-going and was presented:

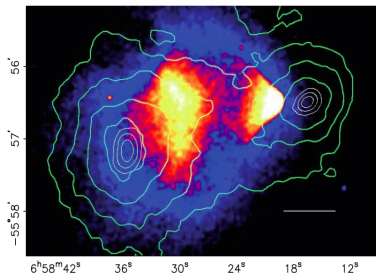
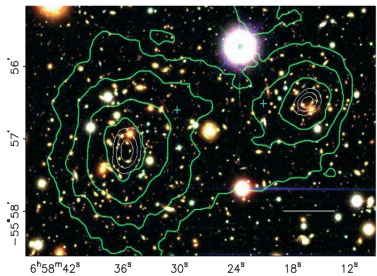
- This search is considering the **Run II legacy dataset** collected by the CMS detector;
- At IFCA, our efforts are entirely focused on the **dilepton final state**;
- This search is performed by defining a ANN, training it to be able to recognize background and signal events, to separate them and **increase the signal efficiency**;
- First time that such a combination will be performed considering this canal, which should increase by a lot the limits published in 2016;
- We expect this analysis **to be approved by June**.

Back up

Gravitational lensing

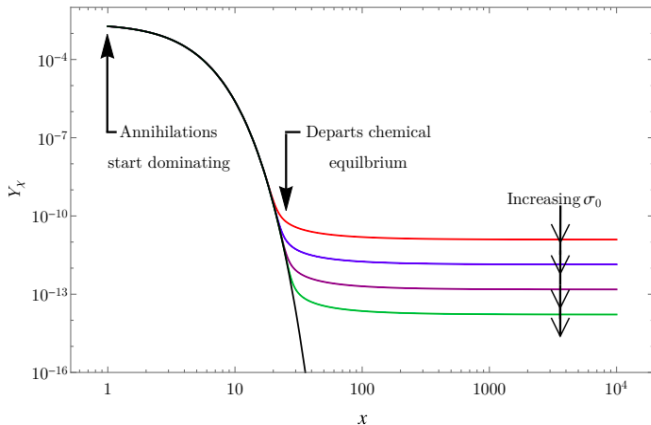
Consequence of the general relativity: massive objects placed between distant sources and the observer should be able to act as lenses and bend the light of the source.

- The deviation of the light is proportional to the mass of the intermediate object, giving us a way to measure its mass;
- The mass distribution obtained has been compared to the luminous distribution of several galaxies, leading to 8σ discrepancies.

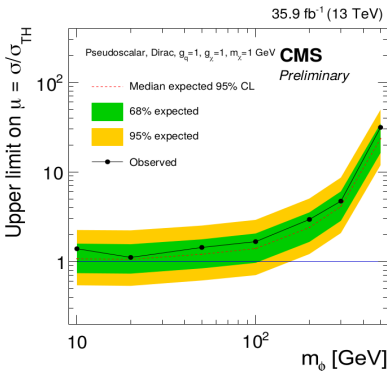
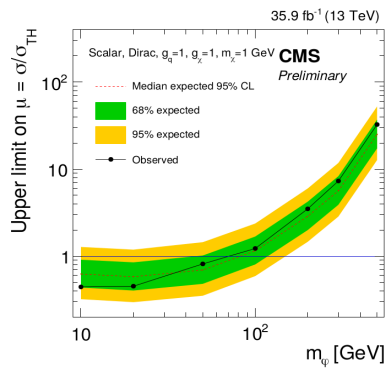


Thermal freeze-out

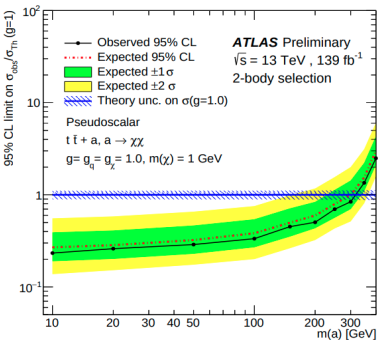
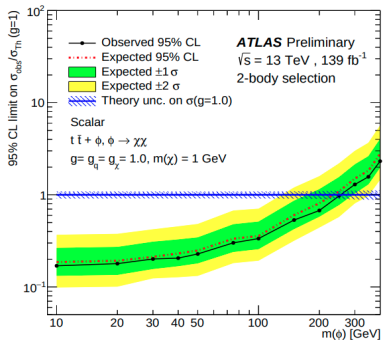
Schematic representation of the freeze-out process, representing the abundance of a 500 GeV dark matter with respect to the time and the impact of increasing cross-section annihilation values on this freeze-out abundance.



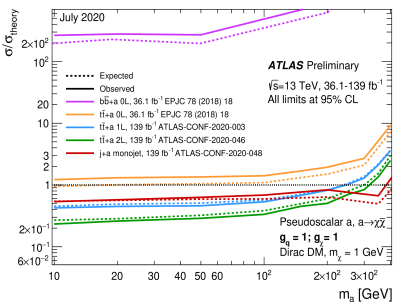
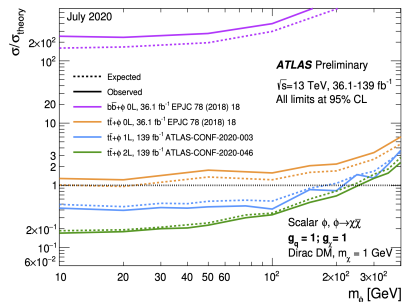
CMS dilepton channel 2016 results published:



ATLAS dilepton channel Run II legacy results from ICHEP 2020:



The ATLAS collaboration does not perform any combination between the different channels though.



Center of mass energy

The center of mass energy is defined as a Lorentz invariant quantity under any kind of boost resulting of the collisions between two protons (defined as E_1, \vec{p}_1, m_1 and E_2, \vec{p}_2, m_2) with a θ angle.

$$\sqrt{s} = \sqrt{(m_1)^2 + (m_2)^2 + 2(E_1 E_2 - 2|\vec{p}_1| |\vec{p}_2| \cos(\theta))}$$

The LHC started its operation in 2008 running at an energy of 7 TeV, quickly moved to 8 TeV and kept this level of energy during the end of the Run I of operation. In 2015, the energy was increased to 13 TeV.

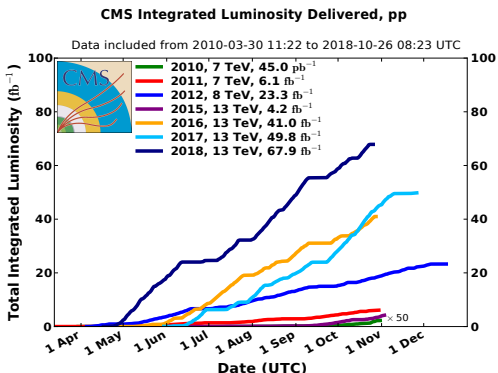
An expected value of 14 TeV, the nominal energy for which the LHC was originally built, is expected to be reached in the near future.

Luminosity

The luminosity \mathcal{L} gives an indication on the number of collisions per second given by the accelerator. Increasing it is crucial to collect as much data as possible, to be able to isolate processes having a low production cross section.

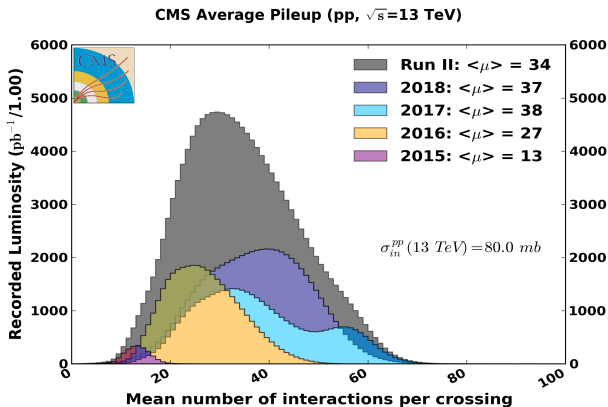
The rate of production R of any given process can be expressed from the instantaneous luminosity $\mathcal{L}(t)$ and the process production cross-section σ :

$$\begin{cases} R = \mathcal{L} \cdot \sigma \\ N(T) = \sigma \int_0^T \mathcal{L}(t) dt = \sigma L \end{cases}$$



Pile-up

Because of the high density of protons within the beams, a bunch crossing in an experiment produces around 30-35 proton collisions.



The Primary Vertex is defined as the most interesting and energetic vertex, while the other vertices are usually referred to as the pile-up.

LHC operational parameters

Key parameters of operation of the LHC, depending on the data-taking period:

| Parameter | Run I | Run II | Run III | Design |
|--|-------|-----------|-----------|--------|
| Energy [TeV] | 7 → 8 | 13 | 13 | 14 |
| Bunch spacing [ns] | 50 | 25 | 25 | 25 |
| Intensity [10^{11} protons per beam] | 1.6 | 1.2 | Up to 1.8 | 1.15 |
| Bunches | 1400 | 2500 | 2800 | 2800 |
| Emittance [μm] | 2.2 | 2.2 | 2.5 | 3.5 |
| β^* [cm] | 80 | 30 → 25 | 30 → 25 | 55 |
| Crossing angle [μrad] | - | 300 → 260 | 300 → 260 | 285 |
| Peak luminosity [$10^{34} \text{ cm}^{-2} \text{ s}^{-1}$] | 0.8 | 2.0 | 2.0 | 1.0 |
| Peak pile-up | 45 | 60 | 55 | 25 |

The tracker is the innermost piece of CMS, able to reconstruct the trajectories of charged particles issued from the interaction vertices in a quick and precise way:

- Needs to be extremely fast to read the 40MHz of collision data, while being resistant to the radiation (expected lifetime ~ 10 years);
- It should be as small as possible to minimize the interaction between the detector and the particles created;
- However, fast electronics usually needs to be cooled down, which increases the size of the subdetector.

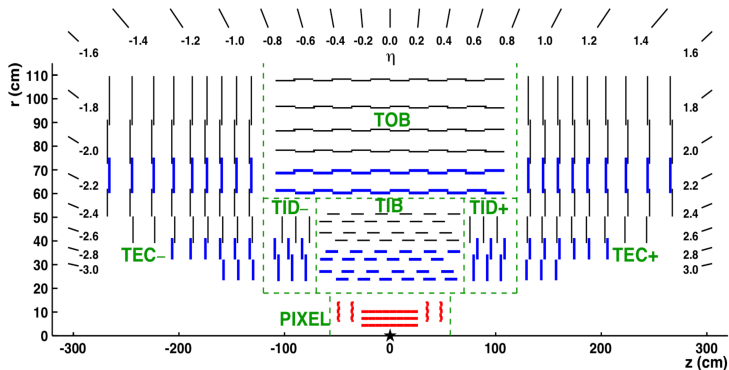
Made out of two main parts:

- The **pixel detector**, made out 60 millions pixels which make up the 1856 active modules of this detector, covering an area of $\sim 1 \text{ m}^2$;
- The **silicon strip detector**, covering an area of $\sim 200 \text{ m}^2$, and made out of three different sub-systems for hermeticity.

A charged particle crossing the tracker will leave a hit each time it crosses one of the silicon sensors, allowing us to reconstruct its track.

The silicon detector is divided into three main parts:

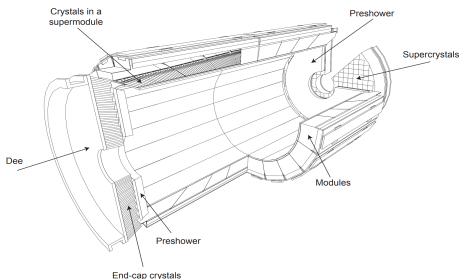
- The Tracker Inner Barrel and Disks (TIB/TBD), using micro-strips parallel in the barrel and perpendicular to the beam axis in the endcaps;
- The Tracker Outer Barrel (TOB), adding 6 measurement layers to the tracker;
- And finally the Tracker EndCaps (TECs), made out of 9 disks, completing the system at high pseudorapidities.



The ECAL is a subdetector sitting inside the solenoid but enclosing the tracker system that gives information about the energy of electrons and photons, both able to interact electromagnetically with its crystals.

Made out of different layers:

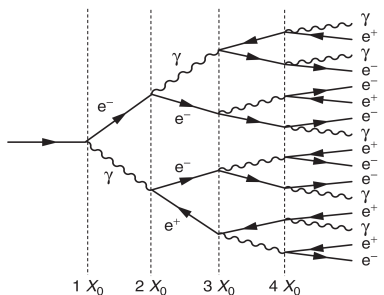
- The barrel part (EB), at $|\eta| < 1.479$, made out of 61 200 lead tungstate (PbWO_4) crystals;
- Two endcaps, each made out of 7 324 crystals, increasing the coverage of the detector up to $|\eta| < 3$;
- The preshower, helping with the identification of electrons against minimum ionizing particles.



The principle of action of the ECAL is simple, and is based on **electromagnetic showers**. When an electron or a photon enters the ECAL, it starts to interact in different ways:

- Photons will mainly produce pairs of electrons and anti-electrons;
- Electrons themselves tend to emit additional photons by bremsstrahlung effect.

This results in a chain reaction during which the incident particle gives most of its energy to the detector, energy measurable using photodetectors and photomultipliers.



Although quite fragile and sensitive to the temperature, the short radiation length X_0 of the PbWO_4 crystals is an advantage, along with their scintillation decay time smaller than the bunch crossing.

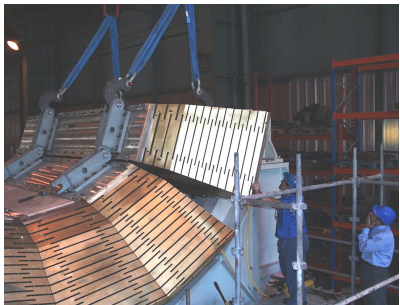
Each crystal measures $2.2 \times 2.2 \times 23 \text{ cm}$, corresponding to 26 radiation lengths.

Charged hadrons lose energy when they traverse matter due to the ionization process resulting from the strong interaction between them and the nuclei of the detector.

Showers of particles are typically produced since the primary hadronic interaction will produce several additional hadrons, themselves interacting even more with the detector.

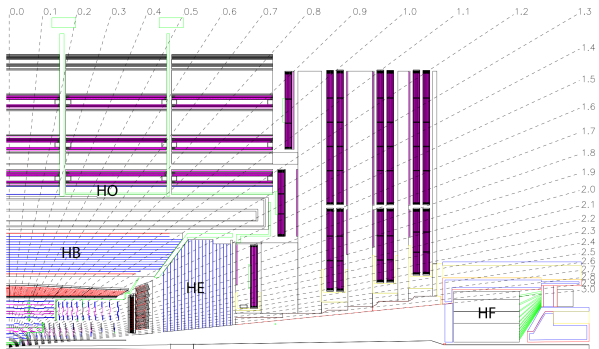
The HCAL is made out of alternating layers:

- Of thick **absorber material**, in which the showers can develop;
- And thin layers of **active material** used for the actual detection by sampling the energy deposition.



The HCAL is divided into:

- A barrel (HB), up to $|\eta| = 1.3$;
- Two endcaps, extending the pseudorapidities coverage up to $|\eta| = 3.0$;
- Two symmetrical forward regions (HF), covering up to $|\eta| = 5.2$;
- And the Hadron Outer (HO), outside of the solenoid, placed to increase the effective nuclear radiation length λ , otherwise low at a 90° incidence angle.



CMS solenoid

The superconducting solenoid:

- Is made out of 6 endcap disks and 5 barrel wheels;
- Weights more than 12 000 tons in total, with the return yoke;
- Is able to produce a 3.8T magnetic field once cooled down to 4.5K;
- Stores around 2.6GJ of energy when active.



It allows the measurement of the momentum and charge of particles by studying the curvature of their tracks, according to the Lorentz equation:

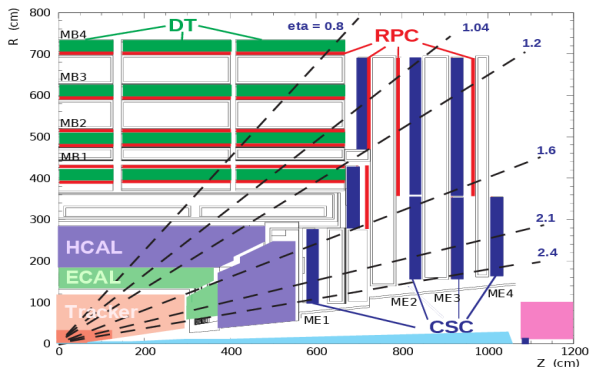
$$\vec{F} = \frac{m\vec{v}^2}{R} = q\vec{E} + q\vec{v} \times \vec{B} = q\vec{v} \times \vec{B}$$

It has been designed to reach a momentum resolution $\Delta p/p \sim 10\%$ at $p = 1$ TeV.

CMS muon systems I

The muon systems is the outermost section of CMS, covering around 25 000 m².

Three different categories of devices have been designed, in order to cope with the specific experimental conditions in the different parts of the detector: the Drift Tubes (DTs), the Cathode Strips Chambers (CSCs), and the Resistive Plate Chambers (RPCs).



All these detectors are gaseous, distributed over a cylindrical area given the shape of the innermost components of CMS, and cheap, given the large surface they cover.

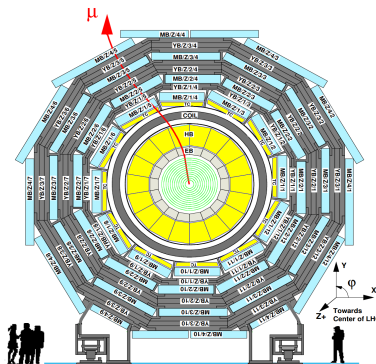
Comparison of the different subsystems:

| Muon sub-system | DTs | CSCs | RPCs |
|-------------------------------|----------------------|--|-------------------------------------|
| $ \eta $ coverage Stations | 0.0-1.2 4 | 0.9-2.4 4 | 0.0-1.9 4 |
| Chambers | 250 | 540 | 480 (barrel) 576 (endcaps) |
| Readout channels | 172 000 | 266 112 (strips) 210 816 (anode channels) | 68 136 (barrel) 55 296 (endcaps) |
| Spatial resolution | 80-120 μm | 40-150 μm | 0.8-1.2 cm |
| Average efficiency (13 TeV) | 97.1% | 97.4% | 94.2% (barrel) 96.4% (endcaps) |

Placed in the barrel region (up to $|\eta| = 1.2$), where the background levels and magnetic field are low, this system allows a good efficiency for the muon hits reconstruction into a single track and a good rejection of eventual background hits.

This system is:

- Able to collect the residuals charges left by the ionization tracks of muons;
- Made out of 172 000 sensitive wires, divided in 250 chambers;
- Redundant, by the installation of 4 layers, to reduce the impact coming from eventual neutrons or photons;
- Has a maximal drift time of 380ns, low enough to avoid the need of multi-hits electronics.



2016 data samples

| Dataset | Events (size) | \mathcal{L} [fb $^{-1}$] |
|--|---------------------|-----------------------------|
| Run 2016B | | |
| /DoubleEG/Run2016B_ver2-Nano02Apr2020_ver2-v1/NANOAOOD | 143073268 (99.4Gb) | |
| /DoubleMuon/Run2016B_ver2-Nano02Apr2020_ver2-v1/NANOAOOD | 82535526 (53.2Gb) | |
| /MuonEG/Run2016B_ver2-Nano02Apr2020_ver2-v1/NANOAOOD | 32727796 (26.8Gb) | 5.8 |
| /SingleElectron/Run2016B_ver2-Nano02Apr2020_ver2-v1/NANOAOOD | 246440440 (167.8Gb) | |
| /SingleMuon/Run2016B_ver2-Nano02Apr2020_ver2-v1/NANOAOOD | 158145722 (96.4Gb) | |
| Run 2016C | | |
| /DoubleEG/Run2016C-Nano02Apr2020-v1/NANOAOOD | 47677856 (35.3Gb) | |
| /DoubleMuon/Run2016C-Nano02Apr2020-v1/NANOAOOD | 27934629 (19.7Gb) | |
| /MuonEG/Run2016C-Nano02Apr2020-v1/NANOAOOD | 15405678 (12.8Gb) | 2.6 |
| /SingleElectron/Run2016C-Nano02Apr2020-v1/NANOAOOD | 97259854 (69.3Gb) | |
| /SingleMuon/Run2016C-Nano02Apr2020-v1/NANOAOOD | 67441308 (42.4Gb) | |
| Run 2016D | | |
| /DoubleEG/Run2016D-Nano02Apr2020-v1/NANOAOOD | 53324960 (39.6Gb) | |
| /DoubleMuon/Run2016D-Nano02Apr2020-v1/NANOAOOD | 33861745 (24.1Gb) | |
| /MuonEG/Run2016D-Nano02Apr2020-v1/NANOAOOD | 23482352 (19.4Gb) | 4.2 |
| /SingleElectron/Run2016D-Nano02Apr2020-v1/NANOAOOD | 148167727 (104.4Gb) | |
| /SingleMuon/Run2016D-Nano02Apr2020-v1/NANOAOOD | 98017996 (61.3Gb) | |
| Run 2016E | | |
| /DoubleEG/Run2016E-Nano02Apr2020-v1/NANOAOOD | 49877710 (37.9Gb) | |
| /DoubleMuon/Run2016E-Nano02Apr2020-v1/NANOAOOD | 28246946 (20.8Gb) | |
| /MuonEG/Run2016E-Nano02Apr2020-v2/NANOAOOD | 22519303 (19.0Gb) | 4.0 |
| /SingleElectron/Run2016E-Nano02Apr2020-v1/NANOAOOD | 117321545 (86.5Gb) | |
| /SingleMuon/Run2016E-Nano02Apr2020-v1/NANOAOOD | 90984718 (58.7Gb) | |
| Run 2016F | | |
| /DoubleEG/Run2016F-Nano02Apr2020-v1/NANOAOOD | 34577629 (26.9Gb) | |
| /DoubleMuon/Run2016F-Nano02Apr2020-v1/NANOAOOD | 20329921 (15.3Gb) | |
| /MuonEG/Run2016F-Nano02Apr2020-v1/NANOAOOD | 16002165 (13.6Gb) | 3.1 |
| /SingleElectron/Run2016F-Nano02Apr2020-v1/NANOAOOD | 70593532 (51.4Gb) | |
| /SingleMuon/Run2016F-Nano02Apr2020-v1/NANOAOOD | 65489554 (42.4Gb) | |
| Run 2016G | | |
| /DoubleEG/Run2016G-Nano02Apr2020-v1/NANOAOOD | 78797031 (61.6Gb) | |
| /DoubleMuon/Run2016G-Nano02Apr2020-v1/NANOAOOD | 45235604 (34.2Gb) | |
| /MuonEG/Run2016G-Nano02Apr2020-v1/NANOAOOD | 33854612 (29.0Gb) | 7.6 |
| /SingleElectron/Run2016G-Nano02Apr2020-v1/NANOAOOD | 153363109 (109.2Gb) | |
| /SingleMuon/Run2016G-Nano02Apr2020-v1/NANOAOOD | 149912248 (94.6Gb) | |
| Run 2016H | | |
| /DoubleEG/Run2016H-Nano02Apr2020-v1/NANOAOOD | 85388734 (67.7Gb) | |
| /DoubleMuon/Run2016H-Nano02Apr2020-v1/NANOAOOD | 48912812 (37.3Gb) | |
| /MuonEG/Run2016H-Nano02Apr2020-v1/NANOAOOD | 29236516 (26.0Gb) | 8.6 |
| /SingleElectron/Run2016H-Nano02Apr2020-v1/NANOAOOD | 128854598 (93.8Gb) | |
| /SingleMuon/Run2016H-Nano02Apr2020-v1/NANOAOOD | 174035164 (110.2Gb) | |

2017 data samples

| Dataset | Events (size) | \mathcal{L} [fb $^{-1}$] |
|---|---------------------|-----------------------------|
| Run 2017B | | |
| /DoubleEG/Run2017B-Nano02Apr2020-v1/NANOAOD | 58088760 (46.6Gb) | |
| /DoubleMuon/Run2017B-Nano02Apr2020-v1/NANOAOD | 14501767 (10.8Gb) | |
| /SingleElectron/Run2017B-Nano02Apr2020-v1/NANOAOD | 60537490 (42.2Gb) | |
| /SingleMuon/Run2017B-Nano02Apr2020-v1/NANOAOD | 136300266 (86.2Gb) | |
| /MuonEG/Run2017B-Nano02Apr2020-v1/NANOAOD | 4453465 (4.1Gb) | |
| Run 2017C | | |
| /DoubleEG/Run2017C-Nano02Apr2020-v1/NANOAOD | 65181125 (53.8Gb) | |
| /DoubleMuon/Run2017C-Nano02Apr2020-v1/NANOAOD | 49636525 (39.5Gb) | |
| /SingleElectron/Run2017C-Nano02Apr2020-v1/NANOAOD | 136637888 (102.5Gb) | |
| /SingleMuon/Run2017C-Nano02Apr2020-v1/NANOAOD | 165652756 (109.5Gb) | |
| /MuonEG/Run2017C-Nano02Apr2020-v1/NANOAOD | 15595214 (15.0Gb) | |
| Run 2017D | | |
| /DoubleEG/Run2017D-Nano02Apr2020-v1/NANOAOD | 25911432 (21.6Gb) | |
| /DoubleMuon/Run2017D-Nano02Apr2020-v1/NANOAOD | 23075733 (18.6Gb) | |
| /SingleElectron/Run2017D-Nano02Apr2020-v1/NANOAOD | 51526710 (38.5Gb) | |
| /SingleMuon/Run2017D-Nano02Apr2020-v1/NANOAOD | 70361660 (47.2Gb) | |
| /MuonEG/Run2017D-Nano02Apr2020-v1/NANOAOD | 9164365 (8.9Gb) | |
| Run 2017E | | |
| /DoubleEG/Run2017E-Nano02Apr2020-v1/NANOAOD | 56233597 (49.8Gb) | |
| /DoubleMuon/Run2017E-Nano02Apr2020-v1/NANOAOD | 51589091 (44.4Gb) | |
| /SingleElectron/Run2017E-Nano02Apr2020-v1/NANOAOD | 102121689 (81.3Gb) | |
| /SingleMuon/Run2017E-Nano02Apr2020-v1/NANOAOD | 154630534 (111.0Gb) | |
| /MuonEG/Run2017E-Nano02Apr2020-v1/NANOAOD | 19043421 (19.2Gb) | |
| Run 2017F | | |
| /DoubleEG/Run2017F-Nano02Apr2020-v1/NANOAOD | 74307066 (67.1Gb) | |
| /DoubleMuon/Run2017F-Nano02Apr2020-v1/NANOAOD | 79756560 (68.0Gb) | |
| /SingleElectron/Run2017F-Nano02Apr2020-v1/NANOAOD | 128467223 (105.2Gb) | |
| /SingleMuon/Run2017F-Nano02Apr2020-v1/NANOAOD | 242135500 (178.3Gb) | |
| /MuonEG/Run2017F-Nano02Apr2020-v1/NANOAOD | 25776363 (26.3Gb) | |

2018 data samples

| Dataset | Events (size) | \mathcal{L} [fb^{-1}] |
|---|---------------------|------------------------------------|
| Run 2018A | | |
| /DoubleMuon/Run2018A-Nano02Apr2020-v1/NANO AOD | 75499908 (62.6Gb) | |
| /EGamma/Run2018A-Nano02Apr2020-v1/NANO AOD | 327843843 (261.8Gb) | |
| /SingleMuon/Run2018A-Nano02Apr2020-v1/NANO AOD | 241608232 (167.7Gb) | 13.5 |
| /MuonEG/Run2018A-Nano02Apr2020-v1/NANO AOD | 32958503 (32.3Gb) | |
| Run 2018B | | |
| /DoubleMuon/Run2018B-Nano02Apr2020-v1/NANO AOD | 35057758 (28.3Gb) | |
| /EGamma/Run2018B-Nano02Apr2020-v1/NANO AOD | 153822427 (123.1Gb) | |
| /SingleMuon/Run2018B-Nano02Apr2020-v1/NANO AOD | 119918017 (82.3Gb) | 6.8 |
| /MuonEG/Run2018B-Nano02Apr2020-v1/NANO AOD | 16211567 (15.8Gb) | |
| Run 2018C | | |
| /DoubleMuon/Run2018C-Nano02Apr2020-v1/NANO AOD | 34565869 (27.6Gb) | |
| /EGamma/Run2018C-Nano02Apr2020-v1/NANO AOD | 147827904 (119.2Gb) | |
| /SingleMuon/Run2018C-Nano02Apr2020-v1/NANO AOD | 110032072 (75.7Gb) | 6.6 |
| /MuonEG/Run2018C-Nano02Apr2020-v1/NANO AOD | 15652198 (15.3Gb) | |
| Run 2018D | | |
| /DoubleMuon/Run2018D-Nano02Apr2020_ver2-v1/NANO AOD | 168605834 (128.6Gb) | |
| /EGamma/Run2018D-Nano02Apr2020-v1/NANO AOD | 751348648 (583.6Gb) | |
| /SingleMuon/Run2018D-Nano02Apr2020-v1/NANO AOD | 513867253 (344.5Gb) | |
| /MuonEG/Run2018D-Nano02Apr2020_ver2-v1/NANO AOD | 71961587 (68.6Gb) | 32.0 |

2016 MC samples

| Process | Sample | Cross section [pb] |
|------------------|--|--------------------|
| Drell-Yan | DYJetsToLL_M-10to50_TuneCUETP8M1_13TeV-madgraphMLM-pythia8 ($H_T < 70$ GeV) | 15810.0 |
| | DYJetsToLL_M-5to50_HT-100to200_TuneCUETP8M1_13TeV-madgraphMLM-pythia8 | 203.3 |
| | DYJetsToLL_M-5to50_HT-200to400_TuneCUETP8M1_13TeV-madgraphMLM-pythia8 | 54.31 |
| | DYJetsToLL_M-5to50_HT-400to600_TuneCUETP8M1_13TeV-madgraphMLM-pythia8 | 5.697 |
| | DYJetsToLL_M-5to50_HT-600toInf_TuneCUETP8M1_13TeV-madgraphMLM-pythia8 | 1.837 |
| | DYJetsToLL_M-50_TuneCUETP8M1_13TeV-madgraphMLM-pythia8 ($H_T < 70$ GeV) | 6077.22 |
| | DYJetsToLL_M-50_HT-70to100_TuneCUETP8M1_13TeV-madgraphMLM-pythia8 | 146.5 |
| | DYJetsToLL_M-50_HT-100to200_TuneCUETP8M1_13TeV-madgraphMLM-pythia8 | 160.7 |
| | DYJetsToLL_M-50_HT-200to400_TuneCUETP8M1_13TeV-madgraphMLM-pythia8 | 48.58 |
| | DYJetsToLL_M-50_HT-400to600_TuneCUETP8M1_13TeV-madgraphMLM-pythia8 | 6.923 |
| | DYJetsToLL_M-50_HT-600to800_TuneCUETP8M1_13TeV-madgraphMLM-pythia8 | 1.717 |
| TTTo2L2Nu | TTTo2L2Nu_TuneCUETP8M2_ttHtranche3_13TeV-powheg-pythia8 | 87.310 |
| | ST_tW_antitop_5f_inclusiveDecays_13TeV-powheg-pythia8_TuneCUETP8M1 | 35.85 |
| Single top | ST_zW_top_5f_inclusiveDecays_13TeV-powheg-pythia8_TuneCUETP8M1 | 35.85 |
| TTToSemiLeptonic | TTToSemilepton_TuneCUETP8M2_ttHtranche3_13TeV-powheg-pythia8 | 364.35 |
| ttV | TTZToLNuNu_M-10_TuneCP5_PSweights_13TeV-amcatnlo-pythia8 | 0.2529 |
| | TTZToQQ_TuneCUETP8M1_13TeV-amcatnlo-pythia8 | 0.5297 |
| | TTWJetsToLNu_TuneCUETP8M1_13TeV-amcatnloFXFX-madspin-pythia8 | 0.2043 |
| | TTWJetsToQQ_TuneCUETP8M1_13TeV-amcatnloFXFX-madspin-pythia8 | 0.4062 |
| VZ | VVTo2L2Nu_13TeV-powheg | 12.178 |
| | WZTo3LNu_TuneCUETP8M1_13TeV-powheg-pythia8 | 4.42965 |
| | WZTo2L2Q_13TeV_amcatnloFXFX_madspin_pythia8 | 5.595 |
| | ZZTo2L2Nu_13TeV_powheg_pythia8 | 0.5640 |
| | ZZTo2L2Q_13TeV_powheg_pythia8 | 3.22 |
| Others | WWW, WWZ, WZZ, ZZZ, WWG | // |

2017 MC samples

| Process | Sample | Cross section [pb] |
|------------------|--|--------------------|
| Drell-Yan | DYJetsToLL_M-10to50_TuneCP5_13TeV-madgraphMLM-pythia8 ($H_T < 100$ GeV) | 15810 |
| | DYJetsToLL_M-4to50_HT-100to200_TuneCP5_13TeV-madgraphMLM-pythia8 | 203.3 |
| | DYJetsToLL_M-4to50_HT-200to400_TuneCP5_13TeV-madgraphMLM-pythia8 | 54.31 |
| | DYJetsToLL_M-4to50_HT-400to600_TuneCP5_13TeV-madgraphMLM-pythia8 | 5.697 |
| | DYJetsToLL_M-4to50_HT-600tolInf_TuneCP5_13TeV-madgraphMLM-pythia8 | 1.837 |
| | DYJetsToLL_M-50_TuneCP5_13TeV-madgraphMLM-pythia8 ($H_T < 70$ GeV) | 6077.22 |
| | DYJetsToLL_M-50_HT-70to100_TuneCP5_PSweights_13TeV-madgraphMLM-pythia8 | 146.5 |
| | DYJetsToLL_M-50_HT-100to200_TuneCP5_13TeV-madgraphMLM-pythia8 | 160.7 |
| | DYJetsToLL_M-50_HT-200to400_TuneCP5_13TeV-madgraphMLM-pythia8 | 48.58 |
| | DYJetsToLL_M-50_HT-400to600_TuneCP5_13TeV-madgraphMLM-pythia8 | 6.923 |
| | DYJetsToLL_M-50_HT-600to800_TuneCP5_13TeV-madgraphMLM-pythia8 | 1.717 |
| | DYJetsToLL_M-50_HT-800to1200_TuneCP5_13TeV-madgraphMLM-pythia8 | 0.7275 |
| | DYJetsToLL_M-50_HT-1200to2500_TuneCP5_13TeV-madgraphMLM-pythia8 | 0.1614 |
| | DYJetsToLL_M-50_HT-2500tolInf_TuneCP5_13TeV-madgraphMLM-pythia8 | 0.003566 |
| TTTo2L2Nu | TTTo2L2Nu_TuneCP5_13TeV-powheg-pythia8 | 87.310 |
| Single top | ST_tW_antitop_5f_inclusiveDecays_TuneCP5_13TeV-powheg-pythia8 | 35.85 |
| | ST_tW_top_5f_inclusiveDecays_TuneCP5_13TeV-powheg-pythia8 | 35.85 |
| TTToSemiLeptonic | TTToSemiLeptonic_TuneCP5_13TeV-powheg-pythia8 | 364.35 |
| ttV | TTZToLLNuNu_M-10_TuneCP5_PSweights_13TeV-amcatnlo-pythia8 | 0.2529 |
| | TTZToQQ_TuneCUETP8M1_13TeV-amcatnlo-pythia8 | 0.5297 |
| | TTWJetsToLNu_TuneCP5_PSweights_13TeV-amcatnloFXFX-madspin-pythia8 | 0.2043 |
| | TTWJetsToQQ_TuneCUETP8M1_13TeV-amcatnloFXFX-madspin-pythia8 | 0.4062 |
| VZ | WWTo2L2Nu_NNPDF31_TuneCP5_PSweights_13TeV-powheg-pythia8 | 12.178 |
| | WZTo3LNu_TuneCUETP8M1_13TeV-powheg-pythia8 | 4.42965 |
| | WZTo2L2Q_13TeV_amcatnloFXFX_madspin_pythia8 | 5.595 |
| | ZZTo2L2Nu_13TeV_powheg_pythia8 | 0.5640 |
| | ZZTo2L2Q_13TeV_amcatnloFXFX_madspin_pythia8 | 3.22 |
| Others | WWW, WWZ, WZZ, ZZZ, WWG | // |

2018 MC samples

| Process | Sample | Cross section [pb] |
|-------------------|--|--------------------|
| Drell-Yan | DYJetsToLL_M-10to50_TuneCP5_13TeV-madgraphMLM-pythia8 ($H_T < 100$ GeV) | 15810 |
| | DYJetsToLL_M-4to50_HT-100to200_TuneCP5_13TeV-madgraphMLM-pythia8 | 203.3 |
| | DYJetsToLL_M-4to50_HT-200to400_TuneCP5_13TeV-madgraphMLM-pythia8 | 54.31 |
| | DYJetsToLL_M-4to50_HT-400to600_TuneCP5_13TeV-madgraphMLM-pythia8 | 5.697 |
| | DYJetsToLL_M-4to50_HT-600tolInf_TuneCP5_13TeV-madgraphMLM-pythia8 | 1.837 |
| | DYJetsToLL_M-50_TuneCP5_13TeV-madgraphMLM-pythia8 ($H_T < 70$ GeV) | 6077.22 |
| | DYJetsToLL_M-50_HT-70to100_TuneCP5_PSweights_13TeV-madgraphMLM-pythia8 | 146.5 |
| | DYJetsToLL_M-50_HT-100to200_TuneCP5_13TeV-madgraphMLM-pythia8 | 160.7 |
| | DYJetsToLL_M-50_HT-200to400_TuneCP5_13TeV-madgraphMLM-pythia8 | 48.58 |
| | DYJetsToLL_M-50_HT-400to600_TuneCP5_13TeV-madgraphMLM-pythia8 | 6.923 |
| | DYJetsToLL_M-50_HT-600to800_TuneCP5_13TeV-madgraphMLM-pythia8 | 1.717 |
| | DYJetsToLL_M-50_HT-800to1200_TuneCP5_13TeV-madgraphMLM-pythia8 | 0.7275 |
| | DYJetsToLL_M-50_HT-1200to2500_TuneCP5_13TeV-madgraphMLM-pythia8 | 0.1614 |
| | DYJetsToLL_M-50_HT-2500tolInf_TuneCP5_13TeV-madgraphMLM-pythia8 | 0.003566 |
| TTTTo2L2Nu | TTTTo2L2Nu_TuneCP5_13TeV-powheg-pythia8 | 87.310 |
| Single top | ST_tW_antitop_5f_inclusiveDecays_TuneCP5_13TeV-powheg-pythia8 | 35.85 |
| | ST_tW_top_5f_inclusiveDecays_TuneCP5_13TeV-powheg-pythia8 | 35.85 |
| TTTToSemiLeptonic | TTTToSemiLeptonic_TuneCP5_13TeV-powheg-pythia8 | 364.35 |
| ttV | TTZToLLNuNu_M-10_TuneCP5_PSweights_13TeV-amcatnlo-pythia8 | 0.2529 |
| | TTZToQQ_TuneCUETP8M1_13TeV-amcatnlo-pythia8 | 0.5297 |
| | TTWJetsToLNu_TuneCP5_PSweights_13TeV-amcatnloFXFX-madspin-pythia8 | 0.2043 |
| | TTWJetsToQQ_TuneCUETP8M1_13TeV-amcatnloFXFX-madspin-pythia8 | 0.4062 |
| VZ | WWTo2L2Nu_NNPDF31_TuneCP5_13TeV-powheg-pythia8 | 12.178 |
| | WZTo3LNu_TuneCP5_13TeV-amcatnloFXFX-pythia8 | 4.42965 |
| | WZTo2L2Q_13TeV_amcatnloFXFX_madspin_pythia8 | 5.595 |
| | ZZTo2L2Nu_TuneCP5_13TeV_powheg_pythia8 | 0.5640 |
| | ZZTo2L2Q_13TeV_amcatnloFXFX_madspin_pythia8 | 3.22 |
| Others | WWW, WWZ, WZZ, ZZZ, WWG | // |

| Mass point | Cross-section [pb] |
|---|-----------------------|
| Scalar mediators | |
| DMscalar_Dilepton_top_tWChan_Mchi1_Mphi10 | $4.959 \cdot 10^{-2}$ |
| DMscalar_Dilepton_top_tWChan_Mchi1_Mphi20 | $3.235 \cdot 10^{-2}$ |
| DMscalar_Dilepton_top_tWChan_Mchi1_Mphi50 | $1.323 \cdot 10^{-2}$ |
| DMscalar_Dilepton_top_tWChan_Mchi1_Mphi100 | $5.633 \cdot 10^{-3}$ |
| DMscalar_Dilepton_top_tWChan_Mchi1_Mphi150 | $3.397 \cdot 10^{-3}$ |
| DMscalar_Dilepton_top_tWChan_Mchi1_Mphi200 | $2.359 \cdot 10^{-3}$ |
| DMscalar_Dilepton_top_tWChan_Mchi1_Mphi250 | $1.720 \cdot 10^{-3}$ |
| DMscalar_Dilepton_top_tWChan_Mchi1_Mphi300 | $1.328 \cdot 10^{-3}$ |
| DMscalar_Dilepton_top_tWChan_Mchi1_Mphi350 | $1.018 \cdot 10^{-3}$ |
| DMscalar_Dilepton_top_tWChan_Mchi1_Mphi400 | $6.717 \cdot 10^{-4}$ |
| DMscalar_Dilepton_top_tWChan_Mchi1_Mphi450 | $4.535 \cdot 10^{-4}$ |
| DMscalar_Dilepton_top_tWChan_Mchi1_Mphi500 | $3.206 \cdot 10^{-4}$ |
| DMscalar_Dilepton_top_tWChan_Mchi1_Mphi1000 | $3.045 \cdot 10^{-5}$ |
| Pseudoscalar mediators | |
| DMpseudoscalar_Dilepton_top_tWChan_Mchi1_Mphi10 | $6.151 \cdot 10^{-3}$ |
| DMpseudoscalar_Dilepton_top_tWChan_Mchi1_Mphi20 | $5.869 \cdot 10^{-3}$ |
| DMpseudoscalar_Dilepton_top_tWChan_Mchi1_Mphi50 | $4.946 \cdot 10^{-3}$ |
| DMpseudoscalar_Dilepton_top_tWChan_Mchi1_Mphi100 | $3.658 \cdot 10^{-3}$ |
| DMpseudoscalar_Dilepton_top_tWChan_Mchi1_Mphi150 | $2.754 \cdot 10^{-3}$ |
| DMpseudoscalar_Dilepton_top_tWChan_Mchi1_Mphi200 | $2.097 \cdot 10^{-3}$ |
| DMpseudoscalar_Dilepton_top_tWChan_Mchi1_Mphi250 | $1.616 \cdot 10^{-3}$ |
| DMpseudoscalar_Dilepton_top_tWChan_Mchi1_Mphi300 | $1.253 \cdot 10^{-3}$ |
| DMpseudoscalar_Dilepton_top_tWChan_Mchi1_Mphi350 | $7.851 \cdot 10^{-4}$ |
| DMpseudoscalar_Dilepton_top_tWChan_Mchi1_Mphi400 | $4.371 \cdot 10^{-4}$ |
| DMpseudoscalar_Dilepton_top_tWChan_Mchi1_Mphi450 | $3.095 \cdot 10^{-4}$ |
| DMpseudoscalar_Dilepton_top_tWChan_Mchi1_Mphi500 | $2.321 \cdot 10^{-4}$ |
| DMpseudoscalar_Dilepton_top_tWChan_Mchi1_Mphi1000 | $2.791 \cdot 10^{-5}$ |

$t\bar{t} + \text{DM}$ signal samples

| Mass point | Cross-section [pb] |
|---|-----------------------|
| Scalar mediators | |
| TTbarDMJets.Dilepton.scalar._LO_TuneCP5_13TeV-madgraph-mcatnlo-pythia8.mChi_1.mPhi_50 | $3.405 \cdot 10^{-1}$ |
| TTbarDMJets.Dilepton.scalar._LO_TuneCP5_13TeV-madgraph-mcatnlo-pythia8.mChi_1.mPhi_100 | $8.027 \cdot 10^{-2}$ |
| TTbarDMJets.Dilepton.scalar._LO_TuneCP5_13TeV-madgraph-mcatnlo-pythia8.mChi_1.mPhi_150 | $2.673 \cdot 10^{-2}$ |
| TTbarDMJets.Dilepton.scalar._LO_TuneCP5_13TeV-madgraph-mcatnlo-pythia8.mChi_1.mPhi_200 | $1.158 \cdot 10^{-2}$ |
| TTbarDMJets.Dilepton.scalar._LO_TuneCP5_13TeV-madgraph-mcatnlo-pythia8.mChi_1.mPhi_250 | $6.020 \cdot 10^{-3}$ |
| TTbarDMJets.Dilepton.scalar._LO_TuneCP5_13TeV-madgraph-mcatnlo-pythia8.mChi_1.mPhi_300 | $3.579 \cdot 10^{-3}$ |
| TTbarDMJets.Dilepton.scalar._LO_TuneCP5_13TeV-madgraph-mcatnlo-pythia8.mChi_1.mPhi_350 | $2.376 \cdot 10^{-3}$ |
| TTbarDMJets.Dilepton.scalar._LO_TuneCP5_13TeV-madgraph-mcatnlo-pythia8.mChi_1.mPhi_400 | $1.443 \cdot 10^{-3}$ |
| TTbarDMJets.Dilepton.scalar._LO_TuneCP5_13TeV-madgraph-mcatnlo-pythia8.mChi_1.mPhi_450 | $9.025 \cdot 10^{-4}$ |
| TTbarDMJets.Dilepton.scalar._LO_TuneCP5_13TeV-madgraph-mcatnlo-pythia8.mChi_1.mPhi_500 | $6.204 \cdot 10^{-4}$ |
| TTbarDMJets.Dilepton.scalar._LO_TuneCP5_13TeV-madgraph-mcatnlo-pythia8.mChi_20.mPhi_100 | $7.993 \cdot 10^{-2}$ |
| TTbarDMJets.Dilepton.scalar._LO_TuneCP5_13TeV-madgraph-mcatnlo-pythia8.mChi_30.mPhi_100 | $8.052 \cdot 10^{-2}$ |
| TTbarDMJets.Dilepton.scalar._LO_TuneCP5_13TeV-madgraph-mcatnlo-pythia8.mChi_40.mPhi_100 | $8.147 \cdot 10^{-2}$ |
| TTbarDMJets.Dilepton.scalar._LO_TuneCP5_13TeV-madgraph-mcatnlo-pythia8.mChi_45.mPhi_100 | $8.319 \cdot 10^{-2}$ |
| TTbarDMJets.Dilepton.scalar._LO_TuneCP5_13TeV-madgraph-mcatnlo-pythia8.mChi_49.mPhi_100 | $8.304 \cdot 10^{-2}$ |
| TTbarDMJets.Dilepton.scalar._LO_TuneCP5_13TeV-madgraph-mcatnlo-pythia8.mChi_51.mPhi_100 | $9.735 \cdot 10^{-4}$ |
| TTbarDMJets.Dilepton.scalar._LO_TuneCP5_13TeV-madgraph-mcatnlo-pythia8.mChi_55.mPhi_100 | $4.835 \cdot 10^{-4}$ |
| Pseudoscalar mediators | |
| TTbarDMJets.Dilepton.pseudoscalar._LO_TuneCP5_13TeV-madgraph-mcatnlo-pythia8.mChi_1.mPhi_50 | $3.440 \cdot 10^{-2}$ |
| TTbarDMJets.Dilepton.pseudoscalar._LO_TuneCP5_13TeV-madgraph-mcatnlo-pythia8.mChi_1.mPhi_100 | $2.164 \cdot 10^{-2}$ |
| TTbarDMJets.Dilepton.pseudoscalar._LO_TuneCP5_13TeV-madgraph-mcatnlo-pythia8.mChi_1.mPhi_150 | $1.414 \cdot 10^{-2}$ |
| TTbarDMJets.Dilepton.pseudoscalar._LO_TuneCP5_13TeV-madgraph-mcatnlo-pythia8.mChi_1.mPhi_200 | $9.773 \cdot 10^{-3}$ |
| TTbarDMJets.Dilepton.pseudoscalar._LO_TuneCP5_13TeV-madgraph-mcatnlo-pythia8.mChi_1.mPhi_250 | $6.753 \cdot 10^{-3}$ |
| TTbarDMJets.Dilepton.pseudoscalar._LO_TuneCP5_13TeV-madgraph-mcatnlo-pythia8.mChi_1.mPhi_300 | $4.808 \cdot 10^{-3}$ |
| TTbarDMJets.Dilepton.pseudoscalar._LO_TuneCP5_13TeV-madgraph-mcatnlo-pythia8.mChi_1.mPhi_350 | $2.742 \cdot 10^{-3}$ |
| TTbarDMJets.Dilepton.pseudoscalar._LO_TuneCP5_13TeV-madgraph-mcatnlo-pythia8.mChi_1.mPhi_400 | $1.409 \cdot 10^{-3}$ |
| TTbarDMJets.Dilepton.pseudoscalar._LO_TuneCP5_13TeV-madgraph-mcatnlo-pythia8.mChi_1.mPhi_450 | $9.302 \cdot 10^{-4}$ |
| TTbarDMJets.Dilepton.pseudoscalar._LO_TuneCP5_13TeV-madgraph-mcatnlo-pythia8.mChi_1.mPhi_500 | $6.618 \cdot 10^{-4}$ |
| TTbarDMJets.Dilepton.pseudoscalar._LO_TuneCP5_13TeV-madgraph-mcatnlo-pythia8.mChi_20.mPhi_100 | $2.166 \cdot 10^{-2}$ |
| TTbarDMJets.Dilepton.pseudoscalar._LO_TuneCP5_13TeV-madgraph-mcatnlo-pythia8.mChi_30.mPhi_100 | $2.164 \cdot 10^{-2}$ |
| TTbarDMJets.Dilepton.pseudoscalar._LO_TuneCP5_13TeV-madgraph-mcatnlo-pythia8.mChi_40.mPhi_100 | $2.162 \cdot 10^{-2}$ |
| TTbarDMJets.Dilepton.pseudoscalar._LO_TuneCP5_13TeV-madgraph-mcatnlo-pythia8.mChi_45.mPhi_100 | $2.180 \cdot 10^{-2}$ |
| TTbarDMJets.Dilepton.pseudoscalar._LO_TuneCP5_13TeV-madgraph-mcatnlo-pythia8.mChi_49.mPhi_100 | $2.151 \cdot 10^{-2}$ |
| TTbarDMJets.Dilepton.pseudoscalar._LO_TuneCP5_13TeV-madgraph-mcatnlo-pythia8.mChi_51.mPhi_100 | $1.993 \cdot 10^{-3}$ |
| TTbarDMJets.Dilepton.pseudoscalar._LO_TuneCP5_13TeV-madgraph-mcatnlo-pythia8.mChi_55.mPhi_100 | $7.750 \cdot 10^{-4}$ |

2016 triggers

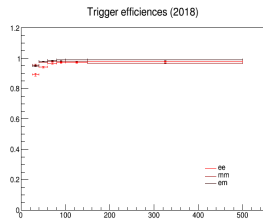
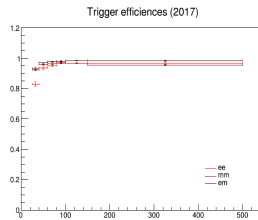
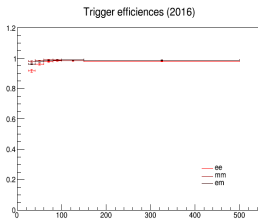
| Dataset | Run range | HLT trigger path |
|-----------|------------------------------------|---|
| Dataset | Run range | HLT trigger path |
| SingleMu | [273158,284044] | HLT_IsoMu24_v* HLT_IsoTkMu24_v* |
| SingleEle | [273158,284044] | HLT_Ele27_WPTight_Gsf_v* HLT_Ele25_eta2p1_WPTight_Gsf_v* |
| DoubleEG | [273158,284044] | HLT_Ele23_Ele12_CaloIdL_TrackIdL_IsoVL_DZ_v* |
| DoubleMu | [273158,281612] [281613,284044] | HLT_Mu17_TrkIsoVVL_Mu8_TrkIsoVVL_v* HLT_Mu17_TrkIsoVVL_TkMu8_TrkIsoVVL_v* HLT_Mu17_TrkIsoVVL_Mu8_TrkIsoVVL_DZ_v* HLT_Mu17_TrkIsoVVL_TkMu8_TrkIsoVVL_DZ_v* |
| MuonEG | [273158,278272] [278273,284044] | HLT_Mu8_TrkIsoVVL_Ele23_CaloIdL_TrackIdL_IsoVL HLT_Mu23_TrkIsoVVL_Ele12_CaloIdL_TrackIdL_IsoVL HLT_Mu12_TrkIsoVVL_Ele23_CaloIdL_TrackIdL_IsoVL_DZ_v* HLT_Mu23_TrkIsoVVL_Ele12_CaloIdL_TrackIdL_IsoVL_DZ_v* |

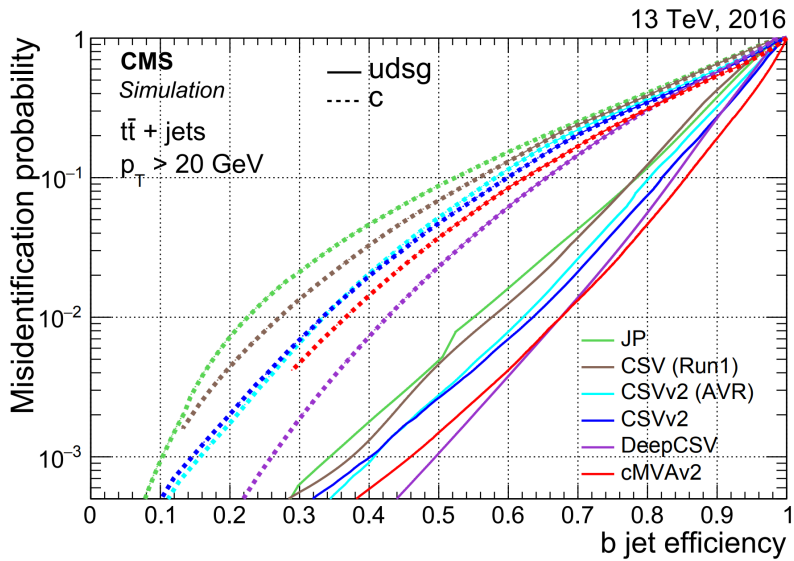
2017 triggers

| Dataset | Run range | HLT trigger path |
|-----------|---|--|
| SingleMu | [297020,306462] | HLT_IsoMu27_v* |
| SingleEle | [297020,306462] | HLT_Ele35_WPTight_Gsf_v* |
| DoubleEG | [297020,306462] | HLT_Ele23_Ele12_CaloIdL_TrackIdL_IsoVL_v* |
| DoubleMu | [297020,299336] [299337,306462] | HLT_Mu17_TrkIsoVVL_Mu8_TrkIsoVVL_DZ_v* HLT_Mu17_TrkIsoVVL_Mu8_TrkIsoVVL_DZ_Mass8_v* |
| MuonEG | [297020,306462] [297020,299336] [299337,306462] | HLT_Mu12_TrkIsoVVL_Ele23_CaloIdL_TrackIdL_IsoVL_DZ_v* HLT_Mu23_TrkIsoVVL_Ele12_CaloIdL_TrackIdL_IsoVL_DZ_v* HLT_Mu23_TrkIsoVVL_Ele12_CaloIdL_TrackIdL_IsoVL_v* |

| Dataset | Run range | HLT trigger path |
|-----------|-----------------|---|
| SingleMu | [315252,325175] | HLT_IsoMu24_v* |
| SingleEle | [315252,325175] | HLT_Ele32_WPTight_Gsf_v* |
| DoubleEG | [315252,325175] | HLT_Ele23_Ele12_CaloIdL_TrackIdL_IsoVL_v* |
| DoubleMu | [315252,325175] | HLT_Mu17_TrkIsoVVL_Mu8_TrkIsoVVL_DZ_Mass3p8_v* |
| MuonEG | [315252,325175] | HLT_Mu23_TrkIsoVVL_Ele12_CaloIdL_TrackIdL_IsoVL_v* |
| | | HLT_Mu12_TrkIsoVVL_Ele23_CaloIdL_TrackIdL_IsoVL_DZ_v* |

Trigger efficiencies computed using orthogonal MET datasets.





MET filters

| Filter name | Applied to data | Applied to simulation |
|---|-----------------|-----------------------|
| Flag_goodVertices | ✓ | ✓ |
| Flag_globalSuperTightHalo2016Filter | ✓ | ✓ |
| Flag_HBHENoiseFilter | ✓ | ✓ |
| Flag_HBHENoiselsoFilter | ✓ | ✓ |
| Flag_EcalDeadCellTriggerPrimitiveFilter | ✓ | ✓ |
| Flag_BadPFMuonFilter | ✓ | ✓ |
| Flag_ecalBadCalibFilterV2 [†] | ✓ | ✓ |
| Flag_eeBadScFilter | ✓ | — |

[†] applied only to 2017 and 2018.

Stransverse mass M_{T2}^{\parallel}

Extension of the transverse mass m_T to cases when pairs of same flavor particles decay into one visible and one invisible particle, such as the double $W \rightarrow l\nu$ decay.

Here, 2 neutrinos contribute to the presence of MET and the individual contribution of each particle ($\not{p}_{T_1}, \not{p}_{T_2}$) to this missing energy cannot be inferred. M_{T2}^{\parallel} is defined as:

$$\begin{cases} M_{T2}^{\parallel} = \min_{\not{p}_{T_1} + \not{p}_{T_2} = \not{p}_{T_{\text{tot}}}} \left(\max \left(m_T^2(\not{p}_{T_1}, \not{p}_{T_1}), m_T^2(\not{p}_{T_2}, \not{p}_{T_2}) \right) \right) \\ m_T^2(\not{p}_T, \not{p}_T) = 4 |\not{p}_T| |\not{p}_T| \sin^2 \left(\frac{\alpha}{2} \right) \end{cases}$$

Different combinations ($\not{p}_{T_1}, \not{p}_{T_2}$) satisfying the condition $\not{p}_{T_1} + \not{p}_{T_2} = \not{p}_{T_{\text{tot}}}$ then need to be probed, keeping only the combination which results in the lowest possible value.

The $t\bar{t}$ process is expected to have an endpoint exactly at the mass of the W boson, while our eventual signal does not have this limitation because of the pair of dark matter particles produced.

m_{bl}^t variable

If a b-jet is produced in a top-quark decay, its invariant mass is bounded from above by $\sqrt{m_t^2 - m_W^2} = 153$ GeV. Events compatible with two semileptonic top-quark decays can then be selected or rejected by introducing the observable m_{bl}^t :

$$m_{bl}^t = \min(\max(m_{l_1 j_a}, m_{l_2 j_b}))$$

In this equation, the minimization is performed either:

- Over all the possible combinations of jets j_a, j_b among the b-jets of the events if three or more j-bets are observed;
- Or over the b-jet(s) observed plus the non b-tagged jet having the highest b-tag weight of the event.

This variable is expected to **give some discrimination** between our two signals of interest.

The spin correlation in a $t\bar{t}$ like event is expected to be conserved, because of the short lifetime of the top quark, and can actually be inferred from the top quark decay products.

Such variables are interesting because **the spin correlation depend on the production mechanism** and will be influenced by the additional coupling to a scalar or pseudoscalar mediator, making this a perfect candidate to be a good discriminating variable.

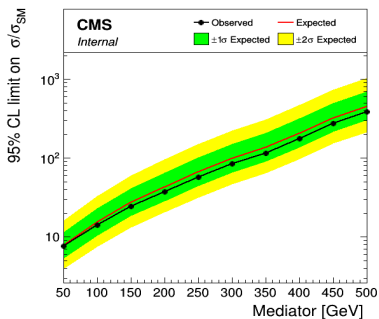
In particular, two spin correlated variables are considered:

- $\xi = \cos(\theta_i) \cos(\theta_j)$, where i and j are either leptons, b-jets or neutrinos;
- $\cos(\Phi_{i,j})$, the cosine of the full opening angle of such top decay products in their respective parent rest frames.

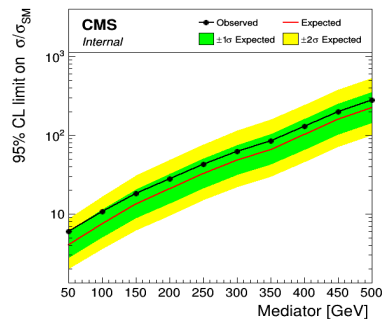
BDT vs ANN

Disclaimer: comparison done without systematics, considering the 2016 with a single 100 GeV training and for a single fb^{-1} of data given the blinding policy applied.

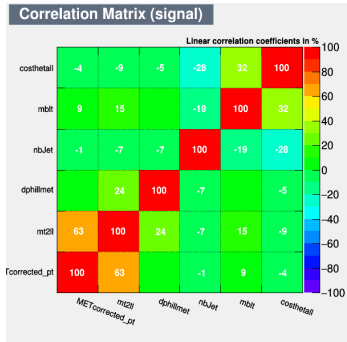
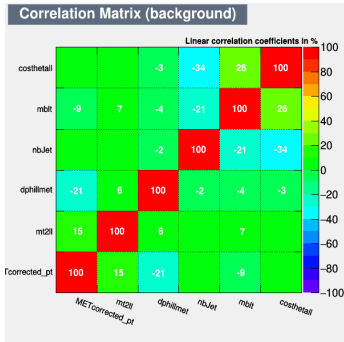
BDT



DNN

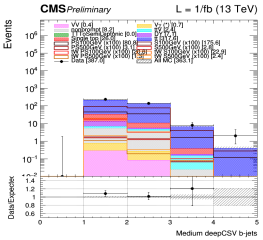
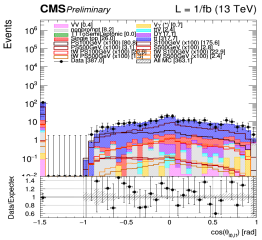
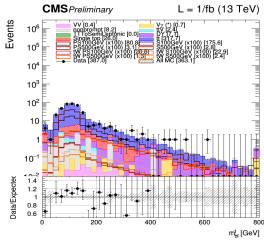
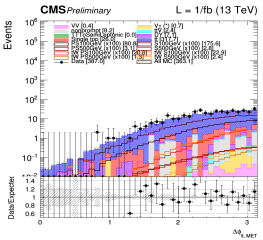
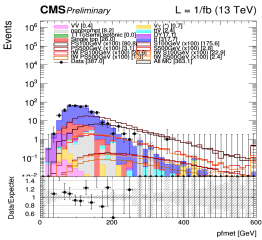
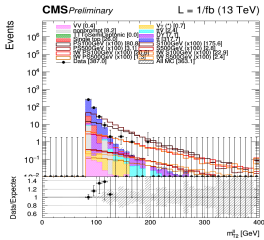


Input variables correlation



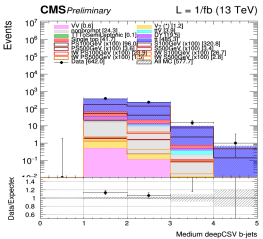
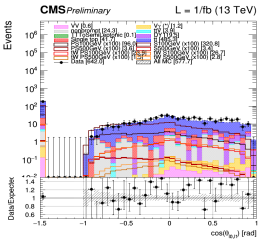
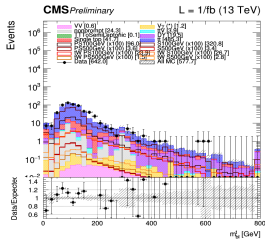
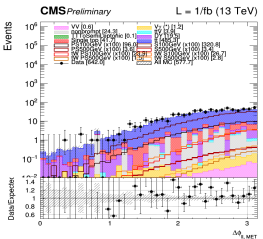
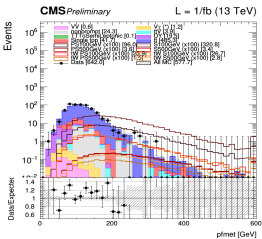
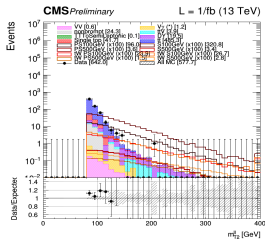
2016 discriminating variables

2016, // channel



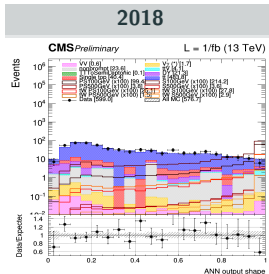
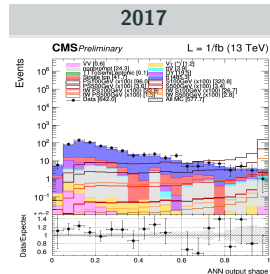
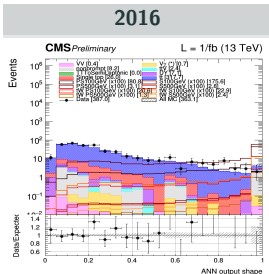
2017 discriminating variables

2017, // channel

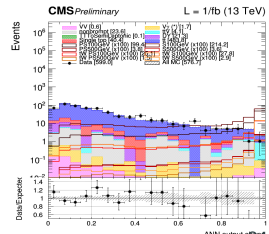
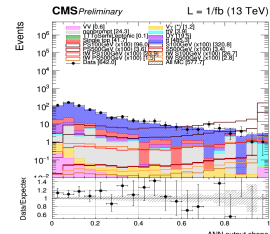
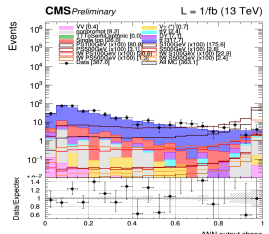


Blinded ANN output shape

Pseudoscalar 100 GeV output shape



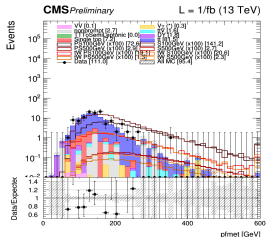
Pseudoscalar 500 GeV output shape



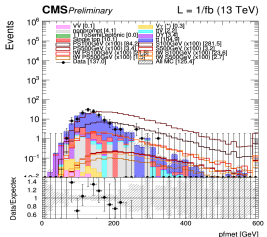
Scalar 100 GeV signal region

// channel

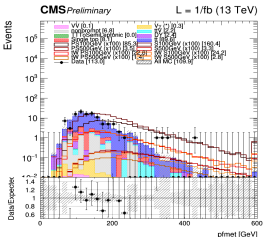
2016



2017



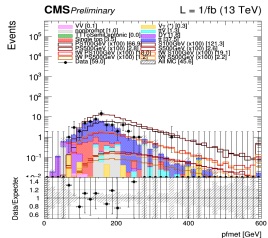
2018



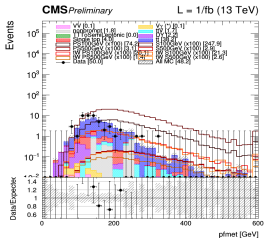
Scalar 500 GeV signal region

// channel

2016



2017



2018

